Monthly Notices
of the
ROYAL ASTRONOMICAL SOCIETY

MNRAS **501,** 2531–2546 (2021)
Advance Access publication 2020 December 12

doi:10.1093/mnras/staa3826

Massive black hole binary inspiral and spin evolution in a cosmological framework

Mohammad Sayeb,[1]★ Laura Blecha,[1]★ Luke Zoltan Kelley,[2]★ Davide Gerosa,[3] Michael Kesden[4] and July Thomas[1]

[1]*Department of Physics, University of Florida, Gainesville, FL 32611, USA*
[2]*Center for Interdisciplinary Exploration and Research in Astrophysics (CIERA), Department of Physics & Astronomy, Northwestern University, Evanston, IL 60201, USA*
[3]*School of Physics and Astronomy and Institute for Gravitational Wave Astronomy, University of Birmingham, Birmingham B15 2TT, UK*
[4]*Department of Physics, University of Texas at Dallas, Richardson, TX 75080, USA*

Accepted 2020 December 7. Received 2020 December 4; in original form 2020 June 9

ABSTRACT

Massive black hole (MBH) binary inspiral time-scales are uncertain, and their spins are even more poorly constrained. Spin misalignment introduces asymmetry in the gravitational radiation, which imparts a recoil kick to the merged MBH. Understanding how MBH binary spins evolve is crucial for determining their recoil velocities, their gravitational wave (GW) waveforms detectable with Laser Interferometer Space Antenna, and their retention rate in galaxies. Here, we introduce a sub-resolution model for gas- and gravitational wave (GW)-driven MBH binary spin evolution using accreting MBHs from the Illustris cosmological hydrodynamic simulations. We also model binary inspiral via dynamical friction, stellar scattering, viscous gas drag, and GW emission. Our model assumes that the circumbinary disc always removes angular momentum from the binary. It also assumes differential accretion, which causes greater alignment of the secondary MBH spin in unequal-mass mergers. We find that 47 per cent of the MBHs in our population merge by $z = 0$. Of these, 19 per cent have misaligned primaries and 10 per cent have misaligned secondaries at the time of merger in our fiducial model with initial eccentricity of 0.6 and accretion rates from Illustris. The MBH misalignment fraction depends strongly on the accretion disc parameters, however. Reducing accretion rates by a factor of 100, in a thicker disc, yields 79 and 42 per cent misalignment for primaries and secondaries, respectively. Even in the more conservative fiducial model, more than 12 per cent of binaries experience recoils of $>500\,\mathrm{km\,s^{-1}}$, which could displace them at least temporarily from galactic nuclei. We additionally find that a significant number of systems experience strong precession.

Key words: gravitational waves.

1 INTRODUCTION

Numerous studies have found a correlation between the masses of massive black holes (MBHs) and the stellar bulges of their host galaxies (e.g. Gültekin et al. 2009; Kormendy & Ho 2013). The origin of these unexpected correlations is still an open question, but galaxy mergers are likely to play a role (Somerville & Davé 2015). A satellite galaxy can gravitationally influence the gas in its host galaxy, and significantly reduce its angular momentum, leading to its infall towards the Galactic Centre (Barnes 1992; Hernquist 1992). This can supply fuel to the MBH (Di Matteo, Springel & Hernquist 2005; Springel, Di Matteo & Hernquist 2005) and may also trigger a burst of star formation around the nucleus (Sanders & Mirabel 1996; Kormendy et al. 2009; Niemi et al. 2012; Hayward et al. 2013).

Galaxy mergers can also lead to the formation of a bound MBH binary (Begelman, Blandford & Rees 1980; Roos 1981). Interactions with stars and gas in the nucleus will shrink the binary's orbit until general relativistic effects become important. At this stage, the binary is driven to merger by gravitational wave (GW) emission.

Crucially, the formation of an MBH binary does not always guarantee merging within a Hubble time. The binary will go through different phases of evolution that can be categorized into four main stages (Begelman et al. 1980). The inspiral is first driven by dark matter (DM), stellar, and gas dynamical friction (DF). At separations of a few parsecs, when a bound binary forms, interactions with individual low angular momentum stars become important. At this stage, the binary loses energy through individual stellar scatterings. Because the range of the available momenta that satisfy the requirement for stellar scattering represents a cone in phase space, this stage is typically referred to as loss-cone (LC) star scattering (Merritt 2013). The stars are scattered out of the system, which removes energy from the MBH binary and shrinks its separation to a few tenths of a pc (Merritt & Rezzolla 2013). In gas-rich systems, further shrinking of the binary separation can happen through gas-driven inspiral where orbital energy and angular momentum are imparted to a circumbinary disc (CBD). Finally, energy loss through GW emission takes over and leads the binary to merger. In general,

★ E-mail: sayebms1@ufl.edu (MS); lblecha@ufl.edu (LB); lzkelley@northwestern.edu (LZK)

at any binary separation, a combination of these mechanisms is at play and determines the merger time-scale and fate of the MBHs (cf. Volonteri et al. 2020).

MBH mergers in the lower mass range of $M \lesssim 10^7$ $M_\odot$ emit GWs at ∼mHz frequencies that can be detected by the future Laser Interferometer Space Antenna (LISA; Amaro-Seoane et al. 2017). Very low frequency (∼nHz) GWs emitted by $M \gtrsim 10^8$ $M_\odot$ MBH binaries are detectable by pulsar timing arrays (PTAs; Sazhin 1978; Detweiler 1979; Mingarelli et al. 2012; Burke-Spolaor 2015; Lommen 2015).

Merging MBH binaries with unequal masses or spins produce asymmetric GW radiation, which in turn imparts a recoil velocity to the remnant MBH (Peres 1962; Bekenstein 1973; Fitchett 1983). Recoils can reduce merger rates (Sesana, Volonteri & Haardt 2009) and affect the growth of MBHs and the co-evolution of the MBH–galaxy system (Blecha & Loeb 2008; Gualandris & Merritt 2008; Volonteri, Lodato & Natarajan 2008; Blecha et al. 2011; Sijacki, Springel & Haehnelt 2011). Large recoil velocities of $\gtrsim$1000 km s^{-1}, produced by some simulations, can even escape massive elliptical galaxies (Schnittman 2007; Gerosa & Sesana 2015). Ejected MBHs might be rare at low redshifts, but in the early universe, with smaller escape speeds and larger merger rates, their frequency might be higher (Volonteri, Haardt & Madau 2003; Madau et al. 2004; Bellovary et al. 2011; Blecha et al. 2016) and could lead to a population of intergalactic MBHs (e.g. Komossa, Zhou & Lu 2008). This is important for the early phase of MBH growth from stellar-mass or intermediate-mass precursors and consequently for the frequency of GW signals and event rates detectable by LISA (Sesana, Volonteri & Haardt 2007). It could also have important repercussions on the observed scatter in the MBH mass and bulge velocity dispersion relations (Libeskind et al. 2006; Gualandris & Merritt 2008; Volonteri et al. 2008; Blecha et al. 2011).

Following an MBH recoil event, the most tightly bound stars and gas will remain with the MBH, while the gas and stars at larger radii will be left behind (Madau & Quataert 2004; Merritt et al. 2004, 2006; Loeb 2007). This can create a relative redshift that can be observed as an offset between broad and narrow lines. One such GW recoil candidate identified was SDSSJ092712.65+294344.0 – an active galactic nucleus (AGN) with a 2650 km s^{-1} shift between its broad and narrow emission lines (Komossa et al. 2008). Further study showed that this effect could be caused by other astrophysical phenomena such as a sub-parsec binary (Bogdanović, Eracleous & Sigurdsson 2009), or a large and small galaxy interacting near the centre of a rich cluster (Heckman et al. 2009). CID-42 is another promising candidate presenting both spatial and spectroscopic offset signatures, but other interpretations are possible (Civano et al. 2010, 2012; Blecha et al. 2013). A growing number of other GW recoil candidates have been identified (Komossa 2012), but none have yet provided unambiguous evidence for a recoiling MBH (Batcheldor et al. 2010; Civano et al. 2010; Robinson et al. 2010; Koss et al. 2014; Chiaberge et al. 2017). The anisotropic emission of linear momentum that causes recoils is imprinted in the emitted GW signals, thus making merger kicks a potential observable for GW interferometers (Gerosa & Moore 2016; Calderón Bustillo et al. 2018; Varma, Isi & Biscoveanu 2020).

In gas-rich systems, a key element is the interaction of the MBHs with their accretion discs (i.e. the CBD phase). There have been extensive studies and simulations of the interactions of MBHs with the circumbinary disc as isolated systems (Artymowicz & Lubow 1996; Natarajan & Pringle 1998; Günther & Kley 2002; MacFadyen & Milosavljević 2008; Perego et al. 2009; Hanawa, Ochi & Ando 2010; Shi et al. 2012; D'Orazio, Haiman & MacFadyen 2013; Farris et al. 2014; Shi & Krolik 2015; Bowen et al. 2017; Ryan & MacFadyen 2017; Tang, Haiman & MacFadyen 2018). The long-standing consensus on gas-rich systems says that higher accretion rates can lead to dynamical torques and viscous drag contributing significantly to shrinking of the binary separation (Begelman et al. 1980; Gould & Rix 2000; Armitage & Natarajan 2002; Escala et al. 2005; MacFadyen & Milosavljević 2008; Haiman, Kocsis & Menou 2009; Lodato et al. 2009; Roedig et al. 2012; Rafikov 2016; Tang, MacFadyen & Haiman 2017). This effect is enhanced in galaxy mergers that drive more gas into the central regions. However, more recent studies show that circumbinary accretion may impart additional angular momentum on the binary and eventually lead to the expansion of the binary separation (Miranda, Muñoz & Lai 2017; Moody, Shi & Stone 2019; Muñoz, Miranda & Lai 2019; Duffell et al. 2020; Muñoz et al. 2020). How broadly applicable these results are to astrophysical binaries is not yet clear.

Recoil velocities depend strongly on pre-merger spins and spin orientations (Campanelli et al. 2007a; González et al. 2007b; Brügmann et al. 2008; Kesden, Sperhake & Berti 2010b; Berti, Kesden & Sperhake 2012; Lousto et al. 2012; Gerosa, Hébert & Stein 2018), which are poorly constrained in both simulations and observations. Gas discs can crucially influence the spins. The interaction of the disc with MBH spin happens mainly via two mechanisms:

(i) In what is known as the Bardeen–Petterson (BP) effect (Bardeen & Petterson 1975), misalignment between the gas disc angular momentum and the MBH spin angle torques the two vectors towards alignment with each other.

(ii) The angular momentum of matter accreted on to the MBH changes the spin of the MBH (King & Kolb 1999).

Many studies implementing the BP effect find that in a gas-rich environment with a coherent gas flow, the MBH in a binary on average spins up and becomes aligned with the disc prior to merger (e.g. Scheuer & Feiler 1996; Martin, Pringle & Tout 2007, 2009; Tremaine & Davis 2014) and, as a result, it experiences smaller recoil velocities (Lousto et al. 2012; Gerosa et al. 2015b). Simulations by Dotti et al. (2010) find that MBH spins align with the angular momentum of their orbit on time-scales of <1–2 Myr. They report typical alignments of ∼10° (∼30°) for cold (warm) discs. 1D simulations reported the existence of critical configurations where the disc is expected to break, potentially leading to larger misalignment angles (Tremaine & Davis 2014; Gerosa, Rosotti & Barbieri 2020). However, spinning up of the MBH might not always be the case. In the case of chaotic accretion, where the matter inflow comes from different directions and at different speeds, the different accretion efficiencies between prograde and retrograde orbits will, on average, spin the black holes down (King & Pringle 2006; Capelo & Dotti 2017). In addition to that even in smooth gas flows, outer annuli can torque inner annuli leading to wild fluctuations in the spin misalignment (Hopkins et al. 2012).

If an MBH binary has misaligned spin when it enters the GW-dominated regime, the spin orientation will be modified by relativistic spin precession. At orbital separations $a \gg GM/c^2$, where M stands for the total mass of the MBH binary, the system can be studied in the post-Newtonian (PN) approximation (e.g. Blanchet 2014; Will 2016). MBH spins precess and orbital energy is lost to GWs on time-scales proportional to $a^{5/2}$ and a^4, respectively (Apostolatos et al. 1994). At separations $a \sim GM/c^2$, the PN approximation breaks down and systems need to be studied using full numerical relativity simulations (e.g. Lehner & Pretorius 2014).

We utilize data from the cosmological hydrodynamic simulation suite Illustris (e.g. Genel et al. 2014; Vogelsberger et al. 2014a,

b; Nelson et al. 2015). The Illustris simulation has successfully reproduced many of the observed properties of galaxies and their MBHs, such as galaxy merger rates, stellar and MBH mass functions, the cosmic star formation rate density, and the baryonic Tully–Fisher relation (Genel et al. 2014; Vogelsberger et al. 2014a; Sijacki et al. 2015). It has also been extensively used for studies of recoiling MBH and MBH binary evolution (Blecha et al. 2016; Kelley, Blecha & Hernquist 2017a; Kelley et al. 2017b, 2018; Katz et al. 2020).

In this paper, we focus on modelling and characterizing the spin evolution of MBHs in a cosmological framework and studying its effects on MBH mergers and recoil velocities. In particular, we study the dependence of spins and recoils on parameters such as the MBH accretion rate and the orbital eccentricity. We also explore how these effects may impact the number of precessing binaries observable by LISA. In this work, we model gas and GW-driven binary MBH spin evolution in a cosmological framework. Our model predicts MBH merger rates with important implications for hierarchical structure formation and galaxy–MBH coevolution.

In Section 2 of this paper, we provide a description of the model. In Section 3, we discuss our findings, including the dependence of MBH binary spin misalignment on initial spin distributions, accretion rates, and eccentricities. We also examine the resulting recoil velocity distributions, as well as the fraction of binaries that should be strongly precessing in the LISA band. In Section 4, we discuss our conclusions.

2 DESCRIPTION OF THE MODEL

For our analysis, we use data from the Illustris project,[1] which is a cosmological hydrodynamic simulation suite that reproduces key observables of galaxy and active galactic nucleus (AGN) populations over cosmic time. Because our focus is on MBH evolution, we primarily utilize the masses, accretion rates, and redshifts of merging MBHs. To evolve binary inspiral below the simulation resolution, we follow the prescription put forward by Kelley et al. (2017a, b), where extrapolated density profiles of the host galaxies are used to estimate the MBH hardening rates in the DF, LC, and CBD stages. The GW-dominated regime is modelled using the PN framework implemented in the PRECESSION code (Gerosa & Kesden 2016). We use PN evolution up to separations of $a = 10GM/c^2$ where we apply fitting formulae derived from numerical-relativity simulations to estimate the properties, including the recoil, of the merger remnant. In order to account for statistical robustness, we have run 10 different realizations of each model. Throughout this paper, we denote the mass of the heavier MBH with m_1, the mass of the lighter companion with m_2, the binary total mass with $M = m_1 + m_2$, and the mass ratio with $q = m_2/m_1 \leq 1$.

2.1 Illustris simulation suite

Cosmological hydrodynamic simulations generally use one of two approaches: (i) smooth particle hydrodynamics (SPH; e.g. Gingold & Monaghan 1977; Lucy 1977) or (ii) an Eulerian mesh-based approach (e.g. Berger & Colella 1989). The Illustris simulation leverages the AREPO code (Springel 2010) which combines the advantages of both Eulerian and SPH approaches based on an unstructured moving mesh. The mesh is formed from a Voronoi tesellation based on a set of discrete mesh-generating seeds that can freely move and create a dynamic topology (Springel 2010).

[1] http://www.illustris-project.org/

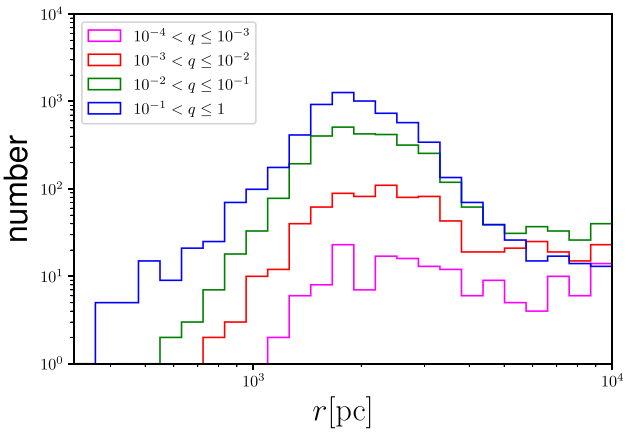

Figure 1. Distribution of gravitational softening lengths for MBH binaries in Illustris. For each binary, the maximum of the softening lengths is taken as the initial binary separation. In the Illustris simulations, MBHs instantaneously merge as they get within a particle softening length of each other. These softening lengths, even at the very small tail, represent values of the order of a few hundred pc, while the GW-driven regime takes place on mpc scales. At these separations, binaries are far from merged. For some of the binaries, it can take more than a Hubble time to go from these large separations down to GW-dominated radii and coalescence depending on the host properties. Therefore, a sub-resolution model is needed in order to understand the binary evolution below the softening lengths where evolution is not resolved by Illustris.

Particles represent stars, DM, and massive MBHs (Vogelsberger et al. 2013, 2014a, b). The MBH particles in Illustris are seeded at a mass of 1.42×10^5 $M_\odot$ and placed in all haloes that have at least a mass of 7.1×10^{10} $M_\odot$ and lack an MBH (Sijacki et al. 2015). The algorithm assigns the highest density gas particle as the MBH and places it at the minimum of the halo potential. After formation, MBHs can grow either through Eddington-limited Bondi accretion or mergers (Di Matteo et al. 2005; Springel et al. 2005). When two MBHs come to within a gravitational softening length of each other, they are merged instantaneously. Computational requirements imply that a gravitational softening length is typically around a few kpc (see Fig. 1) where, in reality, MBHs are still far from merger. Our main focus here is to understand and model the evolution of MBHs and their spins on these sub-resolution scales.

Illustris, like many comological simulations, uses a repositioning scheme to stabilize the MBH dynamics, wherein the MBH is always placed on to the potential minimum of its host halo. Especially for unequal-mass mergers, this might cause MBHs in small satellite haloes to merge with the larger central MBH on unphysically short time-scales. As this primarily affects MBHs near the seed mass, we choose to exclude the population of MBHs with a mass of $M_\bullet < 10^6$ $M_\odot$ for each individual MBH (Blecha et al. 2016; cf. Katz et al. 2020).

The Illustris simulations are run on a cosmological box of side $L_{\rm box} = 75\ h^{-1}$Mpc. Throughout this paper, we use the highest resolution run, 'Illustris-1'. Simulations assume a WMAP9 cosmology with parameters $\Omega_{\rm m} = 0.2865$, $\Omega_\Lambda = 0.7135$, $\sigma_8 = 0.820$, and $H_0 = 70.4$ km s^{-1} Mpc^{-1} (Hinshaw et al. 2013).

2.2 Binary inspiral time-scales

The merger of the MBHs in Illustris marks the initial point of our sub-resolution, post-processing analysis. With our post-processing,

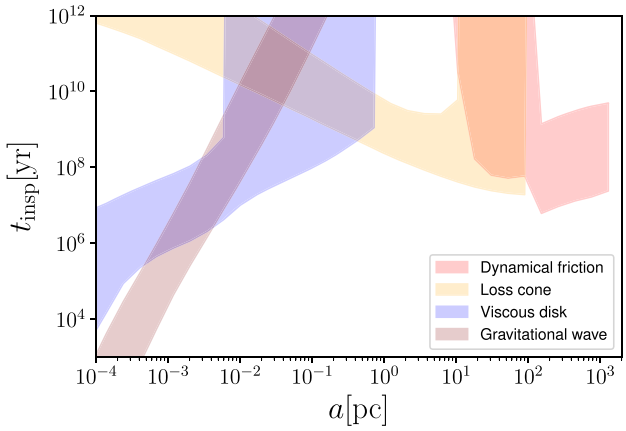

Figure 2. Hardening time-scales for different mechanisms for the middle 50 per cent of the population. DF starts from a few kpc and dominates up to a few pc after which LC takes over up to a few hundredth of a pc. Finally, CBD and GW will dominate the inspiral at smaller separations. For each case the time-scales are found using $a\,(\mathrm{d}a/\mathrm{d}t)^{-1}$, where a is the semimajor axis of the binary.

we have a median inspiral time-scale of ∼8 Giga years for the total population. For the merged systems, the median inspiral time-scale is 1.6 Gyr and for the major mergers ($q > 0.3$) that merge by $z = 0$, the median inspiral time-scale is 1.2 Gyr. After Illustris merger point, we evolve the binaries using the prescription from Kelley et al. (2017a, b). The binary hardening – i.e the shrinking of the binary separation – happens through four different processes: DF, LC, interaction with CBD, and GW radiation.

A moving MBH in a background of DM, gas, and stars will perturb the background by creating a gravitational wake that removes orbital energy from MBH and thermalizes the background. During the early stages of galaxy coalescence, this effect, known as dynamical friction (DF), is the most dominant form of energy dissipation (Antonini & Merritt 2012; Kelley et al. 2017a). The DF calculation follows the change in velocity of a massive object due to an encounter with a single background particle and follows the seminal treatment by Chandrasekhar (1942, 1943). The hardening rate due to the DF is denoted by $(\mathrm{d}a/\mathrm{d}t)_{\rm DF}$. The corresponding inspiral time is estimated as $(t_{\rm insp})_{\rm DF} = a(\mathrm{d}a/\mathrm{d}t)^{-1}_{\rm DF}$. Fig. 2 shows the hardening time-scales due to DF in orange. In particular, we find that DF is the most dominant hardening mechanism for MBH separations larger than a few hundred pc.

From a few hundred pc to a few tenths of a pc, stellar scattering ('Loss Cone' in Fig. 2) typically dominates the MBH inspiral. At this stage, only low angular momentum stars can interact with the binary. Individual scattering events extract energy from the binary by ejecting the star from the system at high velocities. The treatment of LC scattering in Kelley et al. (2017a) is based on models of tidal disruptions from Magorrian & Tremaine (1999) and scattering experiments by Sesana, Haardt & Madau (2008) for circular and eccentric binaries, respectively. The LC hardening rate is denoted by $(\mathrm{d}a/\mathrm{d}t)_{\rm LC}$. The LC hardening rates and hardening time-scales for our population of binaries are shown in Fig. 2 in yellow.

Generally, if there is enough gas, hardening through LC continues until gas accretion on to the MBH binary increases significantly and a circumbinary disc forms. At this stage, CBD hardening can become the dominant mechanism through which the binary loses energy (Begelman et al. 1980; Gould & Rix 2000; Escala et al. 2005). The change in binary separation in the CBD phase is denoted by $(\mathrm{d}a/\mathrm{d}t)_{\rm CBD}$. This effect can be further enhanced following a galaxy merger event where a significant amount of gas is drawn into the centre of the potential. In addition to fuelling accretion on to the MBHs, the CBD phase can drive the rapid inspiral of the binary up to the GW-dominated regime. Our CBD hardening rate is based on the thin-disc model of Shakura & Sunyaev (1973) and follows the prescription by Haiman et al. (2009). In particular, we adopt the basic picture of a binary in a thin circumbinary disc such that the plane of the disc is aligned with the binary orbit. The disc gas density that enters the hardening rate is extracted directly from the accretion rate of the remnant MBH in Illustris (Kelley et al. 2017a).

Accretion rates in Illustris are determined according to the Bondi–Hoyle prescription, capped at the Eddington limit. As described in Vogelsberger et al. (2013) and Sijacki et al. (2015), the accretion rates calculated in the Illustris simulations are derived self-consistently with thermal, radiative, and radio-mode feedback models. In designing the simulations, a small number of free parameters are calibrated to ensure agreement with observations. In particular, by design, the population of MBH from Illustris accurately reproduce the observed masses of MBH in the local universe and also the observed luminosity function of AGN and quasars. Taking these together means that the accretion rates in Illustris are broadly consistent with observations.

The details of the accretion process on small distance scales are unresolved in cosmological simulations. Additionally, the time-scales typically associated with 'steady-state' accretion discs are also unresolved. The behaviour in Illustris can only appropriately be compared to long-duration steady-states in which the local accretion rate (and disc structure) must be consistent with large-scale gas feeding. When accretion rates are low (e.g. $\lambda_{\rm Edd} \ll 1$) the dynamical impact of the disc is also negligible. Because the simulations also enforce an Eddington limit, the relevant range of accretion rates ($\lambda_{\rm Edd} \lesssim 1$) are consistent with a thin disc. Thus, throughout our post-processing analysis of sub-resolution scales, disc surface densities are calculated based on the thin-disc assumption and the accretion rates from Illustris.

The hardening rates and hardening time-scales for the CBD stage are shown in Fig. 2 in blue. For the CBD stage, the outer-edge of the disc is limited by the Toomre stability criterion (as calculated in Haiman et al. 2009).

At separations below a few hundredths of a pc, the binary loses energy mostly through emission of GWs. The rate at which the orbital separation decreases due to gravitational radiation is given by (Peters 1964)

$$\left(\frac{\mathrm{d}a}{\mathrm{d}t}\right)_{\rm GW} = -\frac{64G^3}{5c^5}\frac{m_1 m_2(m_1+m_2)}{a^3}\frac{(1+73e^2/24+37e^4/96)}{(1-e^2)^{7/2}}, \quad (1)$$

where e is the orbital eccentricity. The GW hardening time-scales are estimated as $(t_{\rm insp})_{\rm GW} = a(\mathrm{d}a/\mathrm{d}t)^{-1}_{\rm GW}$, and are shown in brown in Fig. 2.

2.3 Gas-driven spin evolution

A key dynamical effect of the CBD phase is the evolution of MBH spin angular momenta. We study only prograde orbits in the CBD phase, as the complex dynamics that may arise in retrograde CBDs are poorly understood and beyond the scope of this work. The alignment of the individual MBHs with their corresponding discs happens through accretion and relativistic Lens–Thirring precession; this is referred to as the BP effect (Bardeen & Petterson 1975). The MBH spins align with the angular momentum of the inner disc

relatively quickly (on the viscous time) while the outer region remains misaligned, creating a warped profile. The shear forces in the warped inner region will eventually align the outer and inner regions of the disc (Scheuer & Feiler 1996; Lodato & Pringle 2006; Martin et al. 2007; Gerosa et al. 2020). The time it takes for the outer and inner discs to align with each other is given by (Scheuer & Feiler 1996; Natarajan & Pringle 1998; Lodato & Gerosa 2013)

$$t_{\rm al} \simeq 3.4\,\alpha\,\frac{M}{\dot{M}}\left(\frac{\chi}{\alpha_2}\frac{H}{R}\right). \tag{2}$$

Here, M is the MBH mass, $\dot{M}$ is the accretion rate, χ is the dimensionless spin parameter, α is the Shakura & Sunyaev (1973) viscosity parameter, α_2 is the vertical viscosity coefficient, and H/R is the aspect ratio of the disc. For our fiducial model, we assume $\alpha = 0.1$ and $H/R = 10^{-3}$. The value $\alpha_2 \simeq 5.34$ is approximated using the small-warp approximation (Ogilvie 1999).

Tracking in detail the variation of MBH binary spins with time is beyond the scope of this work. Rather, we identify the systems most likely to remain misaligned when they enter the GW regime by comparing the inspiral and alignment time-scales in the CBD phase. Once the spin alignment time-scale $t_{\rm al}$ is calculated, we must compare it with the inspiral time-scales evaluated at the disc radius to determine the degree of misalignment before GW emission takes over. The effective gas disc radius $r_{\rm disc}$ is estimated by comparing the CBD hardening rate to all other rates and determining the location where CBD becomes the dominant process. In other words, $r_{\rm disc}$ is defined as the largest separation at which $\dot{a}_{\rm CBD} > \dot{a}_i$ where i stands for DF, LC, and GW. This prescription gives us disc radii that range from $\sim 10^{-3}$ to 1 pc. If the BP spin alignment time is longer than the gas-driven inspiral time-scale, we assume a 'misaligned' spin distribution at the start of the GW regime, and in the opposite case we assume an 'aligned' distribution, described below.

The total number of binaries in our analysis is 9234, and this prescription yields 19 per cent (1723 binaries) binaries without a CBD-dominated phase. The median value of the total gas fraction of the galaxies hosting these binaries in the Illustris simulation is $\sim$0.33, while the gas-dominated binaries have a median gas fraction of $\sim$0.43. Gas fraction is defined as the ratio of the gas mass over gas and stellar mass and its estimated at the time of spontaneous merger in the Illustris simulation. Gas-dominated binaries tend to have a density profile that allows them to accrete more. The smaller accretion rate in binaries with no CBD-dominated phase means the BP spin alignment is unlikely to work efficiently. For simplicity, we model them as having an isotropic spin distribution. For the rest of the population, we find the spin distribution by comparing their alignment time-scales with the corresponding total inspiral time-scale

$$t_{\rm insp} = \frac{a}{\dot{a}_{\rm tot}}, \tag{3}$$

where $\dot{a}_{\rm tot} = \dot{a}_{\rm DF} + \dot{a}_{\rm LC} + \dot{a}_{\rm CBD} + \dot{a}_{\rm GW}$.

Accretion rates on to the individual MBH are not resolved by the Illustris simulation; only the accretion on to the combined binary system $\dot{M}_{\rm bin}$ are available. Upon formation of a circumbinary disc, the torques from the binary can create a gap in the circumbinary disc with a mass pile-up on the inner edges of the disc. The mass that is accreted on to the gap will then accrete on to the MBHs, creating circumprimary and circumsecondary discs.

Simulations of the dynamics of gas accretion on to the binary have shown a strong correlation between the accretion rates and mass ratio q (Savonije, Papaloizou & Lin 1994; Hayasaki, Mineshige & Ho 2008; MacFadyen & Milosavljević 2008; D'Orazio et al. 2013; Farris et al. 2014; Miranda et al. 2017; Muñoz et al. 2019). For small-mass ratios, the less massive secondary will orbit closer to the edge of cavity and clear away most of the matter falling into the gap. However, if the mass ratio is too small ($q \lesssim 0.03$) the secondary's accretion will not be strong enough to curb the primary's accretion rate (cf. Duffell et al. 2020). Therefore, accretion on to the primary is favoured for $q \to 0$. Our models neglect possible modulations in accretion rate due to non-zero eccentricity, as discussed by e.g. Muñoz & Lai (2016). For larger mass ratios, symmetry implies that matter falls roughly equally on to each MBH. These combined effects have been referred to as 'differential accretion' (Gerosa et al. 2015b).

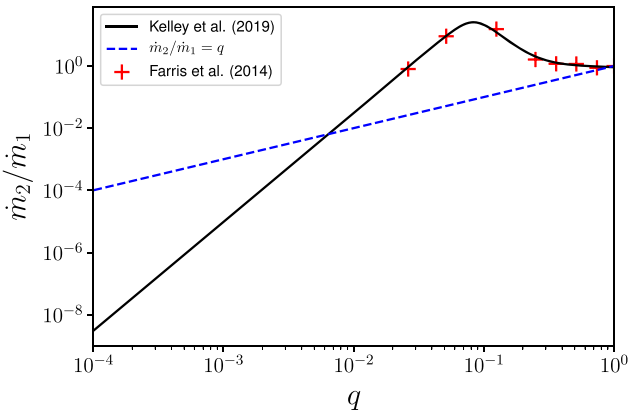

Figure 3. In a circumbinary disc, the differential accretion on to the primary and the secondary MBH is modelled using numerical simulations by Farris et al. (2014) (red crosses) as fitted by Kelley et al. (2019) (dashed curve, equation 4). The relative accretion rate between the primary and the secondary MBH has a strong dependence on the mass ratio q. For more extreme mass ratios, the secondary MBH orbits closer to the edge of the cavity therefore accreting most of the incoming material. Mass ratios closer to unity will reduce the asymmetry and lead to similar accretion rates on to both holes. Accretion rates above the blue dashed line will act to symmetrize the binary.

The ratio $\dot{m}_2/\dot{m}_1$ of the accretion rates is estimated using simulations by Farris et al. (2014) (red crosses in Fig. 3) as fitted by Kelley et al. (2019) (dashed line)

$$\frac{\dot{m}_2}{\dot{m}_1} = q^{a_1} e^{-a_2/q} + \frac{a_3}{(a_4 q)^{a_5} + (a_4 q)^{-a_5}}, \tag{4}$$

where $a_1 = -0.25$, $a_2 = 0.1$, $a_3 = 50$, $a_4 = 12$, and $a_5 = 3.5$ (cf. Gerosa et al. 2015b for a different fit). We assume that all of the matter from the cirumbinary disc accretes on to either of the two MBH, i.e. $\dot{M}_{\rm bin} = \dot{m}_1 + \dot{m}_2$ (but see D'Orazio et al. 2013; Ragusa, Lodato & Price 2016). The individual accretion rates for primary and secondary found here are used in equation (2) to evaluate the alignment time-scales.

Following the CBD evolution, the MBHs reach the final stage of merger, which is dominated by GW emission. The spin distributions found by differential accretion constitute the initial conditions for our PN integrations.

2.4 Spin distributions

The spins of the MBHs prior to merger strongly depend on the accretion rates in the CBD phase (see Shapiro 2005; Volonteri et al. 2005; Barausse 2012, for more on the accretion and spin relations). A binary with a high accretion rate in a gas driven phase will affect the alignment of the spins with the disc through the Bardeen–Petterson effect, leading to a higher degree of alignment of spins with the

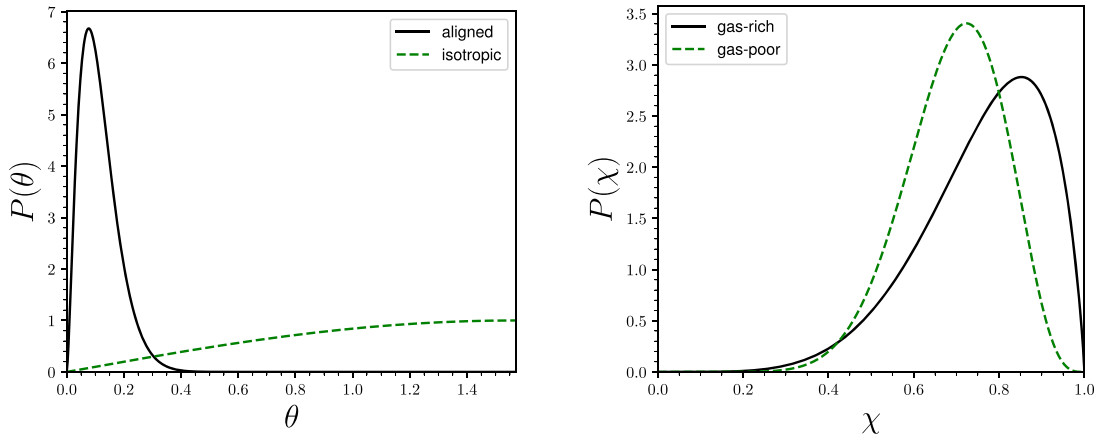

Figure 4. Spin orientation (left) and magnitude (right) distributions used in this paper. For the aligned distribution (cf. Dotti et al. 2010), accretion is assumed to be efficient and spins are close to aligned with the orbital angular momentum. The isotropic distribution, representing successive dry mergers, assigns random spin orientations (Blecha et al. 2016). The fiducial model uses a combination of these, to assign spin directions, based on a comparison between inspiral and spin-alignment time-scales. Coherent accretion is also assumed to spin-up the MBHs to relatively high spin magnitudes depending on the gas richness of the host. In the fiducial model, dimensionless spin parameters are extracted from beta distributions that peak around 0.7 and 0.8 for gas-poor and gas-rich haloes. Gas richness of the halo is based on the gas fraction which is defined as the ratio of the gas mass over total baryonic mass. If the alignment time-scale is larger than the inspiral time-scales, we assume that the MBH remains misaligned by the end of inspiral, and in the fiducial model, these spin directions are assigned from the isotropic distribution. When inspiral time-scales are larger than alignment time-scales, the MBHs are assigned spin directions from the aligned distribution. The assignment of the spin magnitudes χ (i.e. dimensionless spin parameter) is based on the gas fraction of the remnant halo. For gas fractions above and below 0.2 gas-poor and gas-rich distributions are assigned, respectively.

orbital angular momentum vector. In particular, the spin magnitude will increase as $\mathrm{d}\chi/\mathrm{d}t \propto \dot{M}$. It is important to note that the time-scales at which the spin magnitude changes are much larger than the time-scales for spin alignment (Volonteri et al. 2005). This is because in the BP effect, spin alignment is set by the dynamics of the disc warped region, while the spin magnitudes rate is set by the material flowing through the BH innermost stable circular orbit. Also, for a significant change in the spin magnitude, the MBH needs to accrete of the order of its own mass (Bardeen 1970; King & Kolb 1999). Given these considerations, we do not evolve the spin magnitude of the MBHs in this work.

Let us denote with θ_1 and θ_2, the angles between the MBH spins and the orbital angular momentum of the disc. Note that we assume both of the MBH are lying on the plane of the disc. The different time-scales involved imply that we cannot use the same prescription for spin alignment and spin magnitudes.

The distribution of χ is informed by the host galaxy properties. Specifically, we use the total gas fraction of the remnant galaxy assuming that a higher gas fraction will lead to a more coherent flow that spins up the MBH. The gas fraction is defined as the ratio of the gas mass to the total baryonic mass of the galaxy. We develop two distributions for χ, which we dub as 'gas-rich' and 'gas-poor' as shown in the right-hand panel of Fig. 4. The 'gas-poor' case represents a scenario that could be due to the MBH going through successive dry mergers with randomly oriented spins. In this case, the dimensionless spin parameter is extracted from a beta distribution that peaks at ∼0.7 (Blecha et al. 2016). On the other hand, the 'gas-rich' scenario represents a case where accretion is more efficient at spinning up the MBH. In the 'gas-rich' case, the dimensionless spin parameter is extracted from a beta distribution that peaks at ∼0.8.

We choose a critical gas fraction of 0.2 as our gas richness criterion. MBH binaries in haloes with higher gas fractions are assigned spin magnitudes based on the 'gas-rich' distribution, and MBH spin magnitudes in gas-poor haloes are assigned based on the 'gas-poor' distribution. While this choice is arbitrary, we find that our results do not depend strongly on this choice. In other words, a population that is fully assigned a 'gas-rich' distribution or a 'gas-poor' distribution to its spin magnitudes give very similar misalignment percentages and recoil velocity curves.

We also develop two distributions 'aligned' and 'isotropic' for the spin directions θ_i. These distributions are shown on the left-hand panel of Fig. 4. In the 'aligned' case accretion is more coherent and the spins are more closely aligned with the orbital angular momentum vector (Dotti et al. 2010). On the other hand, the 'isotropic' case represents dry mergers with less efficient spin alignment. In our analysis, we are not evolving the spin vectors but rather using a time-scale analysis to assign distributions. For the spin directions, we compare inspiral and alignment time-scale at $r_{\rm disc}$ and assign spin direction based on them. The following is a summary of our model:

$$\begin{cases} P(\chi): & f_{\rm gas} > 0.2 \quad \text{gas-rich} \\ & f_{\rm gas} < 0.2 \quad \text{gas-poor} \\ P(\theta): & t_{\rm al} > t_{\rm insp} \quad \text{misaligned} \\ & t_{\rm al} < t_{\rm insp} \quad \text{aligned} \end{cases} \tag{5}$$

$P(\chi)$ and $P(\theta)$ denote the χ and θ distributions. $f_{\rm gas}$ indicates the gas fraction of the host halo. $t_{\rm insp}$ and $t_{\rm al}$ are inspiral and alignment time-scales, respectively, in the gas-driven inspiral phase. Our distributions for both spin magnitude and directions are shown in Fig. 4.

2.5 Gravitational-wave driven evolution

In the GW-dominated stage, we follow the binary evolution using a PN approach. We make use of the PYTHON module PRECESSION (Gerosa & Kesden 2016). In particular, precession-averaged integrations (Gerosa et al. 2015a; Kesden et al. 2015) allow us to evolve the binary orbital angular momentum and the BH spins directly from the large separations predicted by the previous CBD or LC phase. The code assumes black hole binaries on circular orbits. The treatment is accurate up to 2PN in spin precession and 1.5PN in radiation reaction. Integrations are initialized at the separations

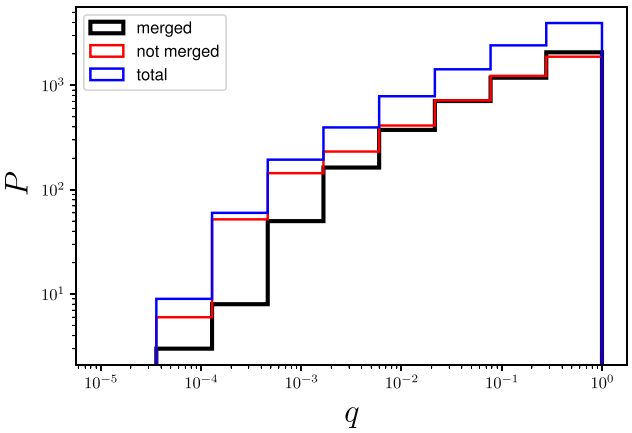

Figure 5. Distribution of mass ratios q for the total population (blue), as well as the merged (black) and non-merged (red) binaries by $z = 0$. The merged population is made of 4451 binaries out of a total sample of 9234. The merged population is skewed towards higher mass ratios.

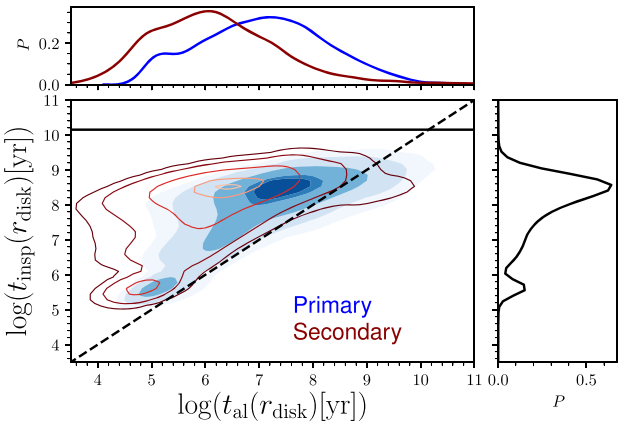

Figure 6. Gas-driven inspiral and BP alignment time-scales for the fiducial model, calculated from the point at which gas-driven inspiral begins to dominate the binary hardening ($r_{\rm disc}$). The blue filled and red line contours indicate primary and secondary MBH's alignment time-scales and they correspond to 99 (outermost contour), 97, 90, 80, and 77 per cent (innermost contour) of the probability distribution function, respectively. Differential accretion along with the smaller mass of the secondaries, imply that primaries take longer than the secondaries to align. The solid horizontal line indicates the Hubble time, while the dashed line denotes equal alignment and inspiral times. In our fiducial model, most MBH spins are aligned by the end of the gas-driven phase, but a non-negligible fraction remains misaligned as they enter the GW-dominated phase.

where GWs start dominating the hardening rate. Precession-averaged evolution is performed down to a final separation of $a = 10GM/c^2$ at which the final angles θ_i and $\Delta\Phi$ are calculated assuming random precessional phases. (The spin magnitudes are constant to very high PN order; see Gerosa et al. 2015a; Kesden et al. 2015 for details). The initial values of θ_1 and θ_2 are provided by the previous (typically CBD) phase, while the initial angle $\Delta\Phi$ between the spin components in the orbital plane is assumed to be randomly distributed in $[-\pi, \pi]$.

Following the precession averaged evolution, the final values of the parameters are used to evaluate fitting formulae to numerical relativity simulation and estimate the properties of the post-merger MBH. In particular, the recoil fit is calibrated on simulations by Campanelli et al. (2007b), González et al. (2007a), Lousto & Zlochower (2008, 2013), Lousto et al. (2012) as collected by Gerosa & Kesden (2016).

3 RESULTS

3.1 Fiducial model

Fig. 6 shows the gas-driven MBH binary inspiral versus spin alignment time-scales, calculated at the start of the CBD phase ($r_{\rm disc}$). We assume all binaries have an initial eccentricity of 0.6 in the fiducial model; our treatment of fixed initial eccentricities follows that in Kelley et al. (2017b, 2018). The eccentricity is assigned at beginning of DF phase, however, it only changes in LC and GW-dominated phases in our model. Eccentricity would also greatly affect accretion on to the MBH binary and the differential accretion but we do not take this into account in our model. Nevertheless, the choice of eccentricity does not significantly affect our final result, as discussed in Section 3.3. In the GW-dominated phase, the hardening rate is strongly dependent on the eccentricity: $t_{\rm insp} \propto (1 - e^2)^{7/2}$, see equation (1). Higher eccentricities will in principle enhance the GW hardening rates and reduce the time to MBH merger. However, in our fiducial model with initial eccentricity of 0.6, we find only 1.7 per cent binaries, that do not have a GW-dominated phase. These rare binaries all accrete at the Eddington rate in their final stages and have unusually high CBD hardening rates; some also have unusually low GW hardening rates.

Fig. 5 shows the mass ratio for merging and non-merging MBH binaries in our model. During the evolution, we calculate the redshift at each step of evolution and the merged binaries are the ones that merge by redshift $z = 0$. The ones that do not merge have inspiral time-scales larger than a Hubble time. The binaries that do not merge are omitted in the GW regime since they do not contribute to the merger rate. Thus they are not contributing to LISA merger rates either. Fig. 5 also shows that the mass ratios for the merged population is skewed towards larger mass ratios ($q > 0.1$). This combined with the differential accretion (Section 2.3), implies that the accretion rate is typically dominated by the secondary MBH. This leads to larger misalignment time-scales for the primary, as seen in Fig. 6. Given the smaller mass of the secondary, with the higher accretion rates caused by differential accretion, its spin alignment is further enhanced. In particular, we find that 19 per cent of the primaries and 10 per cent of the secondaries are misaligned at the end of the CBD phase. Differential accretion in the CBD phase can also drive the binary towards $q = 1$. However, the total accretion in the CBD phase is not enough to significantly change the mass ratio distribution (cf. Siwek, Kelley & Hernquist 2020). Therefore, we make the simplifying assumption of constant mass ratios.

The comparison between inspiral and alignment time-scales (Fig. 6) dictates the configuration of spin orientations at the onset of the GW phase. This effect can be seen in the 'initial' configurations in Fig. 7, which shows that primary MBHs (red curve) are, on average, more misaligned than secondaries (blue curve).

These distributions of θ_1 and θ_2, along with an isotropic distribution of the angle $\Delta\Phi$ between the spin components in the orbital plane, provide the initial conditions to track the BH spins in the GW-driven phase. As shown in Fig. 7, the distribution of polar angles for the primary MBHs does not change significantly during this phase. Its important to point out that individual spins can and do change greatly, even though the overall distribution varies little. Relativistic spin–spin couplings imply that the behaviour of the secondary MBH

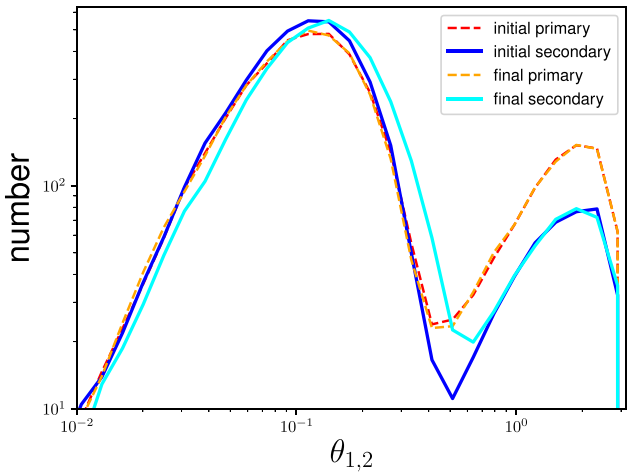

Figure 7. Initial and final angles between MBH spins and the binary orbital angular momentum in the GW-dominated phase, for both primary (red, yellow) and secondary (blue, cyan) MBHs. These polar angles $\theta_{1,2}$ are initialized at the start of the GW-phase based on a comparison between inspiral and alignment time-scales, as shown in Fig. 6. For misaligned spins ($t_{\rm al} > t_{\rm insp}$), spin orientations are assigned from an isotropic distribution, and for $t_{\rm al} < t_{\rm insp}$, spins are assigned from the 'aligned' (partially aligned) distribution as discussed in Section 2.4. Although GR precession can induce large changes in individual spin angles, the overall distribution remains similar, with a slight increase in the misalignment of the initially aligned secondary MBH spins.

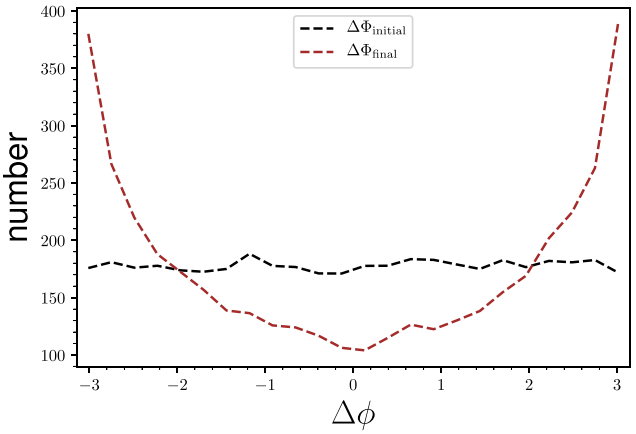

Figure 8. Initial and final distributions of the angle $\Delta\Phi$ between the spin components in the orbital plane during the GW-dominated phase. The initial distribution is determined at the onset of GW-dominated phase (i.e. end of disc phase). Since the disc phase does not affect $\Delta\Phi$, its distribution at the beginning of GW phase is isotropic. However, in the GW-dominated phase, MBH spin precession drives the distribution towards $\Delta\Phi = \pm\pi$ when the secondary spin is aligned, as is the case for 90 per cent of the mergers listed in Table 1.

spin is affected by the primary MBH spin. In systems where the primary MBH spin is misaligned with the orbital angular momentum, relativistic precession tends to induce greater misalignment in the secondary. Conversely, if the primary MBH spin is nearly aligned and the secondary is misaligned, spin precession tends to drive the secondary into greater alignment. In other words, the trend is such that as the separation of angles decreases: the configuration of polar angles tends to go towards $\cos\theta_1 \simeq \cos\theta_2$ (cf. Schnittman 2004; Gerosa et al. 2013; Mould & Gerosa 2020). Isotropic spin distributions tend to remain isotropic during this phase (Bogdanović, Reynolds & Miller 2007). The anisotropic distributions, however, are more significantly affected by relativistic precession (Schnittman 2004; Kesden, Sperhake & Berti 2010a; Gerosa et al. 2015a; Kesden et al. 2015) where the modification of angles before the merger is stronger.

Although spin precession does not dramatically impact the distribution of polar angles θ_1 and θ_2 for our fiducial model, it does strongly affect the distribution of differences in azimuthal angles $\Delta\Phi$ as shown in Fig. 8 (see Kesden et al. 2010b). This occurs because the BP effect aligns the secondary spin in 90.02 per cent of our mergers, and MBHs with aligned spins and mass ratios $q \lesssim 0.5$ are preferentially driven into the $\Delta\Phi = \pm\pi$ librating spin morphology during the GW-driven phase of the inspiral (Gerosa et al. 2015a).

MBHs in this librating spin morphology should have higher kicks because they are closer to the asymmetric 'superkick' configuration (Campanelli et al. 2007a), but we find that precession has a negligible effect on the median recoils for the eight sub-populations in Table 1. This may be an artefact of the bimodal distributions of the spin directions θ_i in Fig. 7; $\Delta\Phi$ is undefined and thus irrelevant in the limit that one or both of the spins is aligned, while distributions in which both spins are initially isotropic remain isotropic throughout the GW-driven phase (Bogdanović et al. 2007).

However, precession can significantly affect individual velocities (Kesden et al. 2010b; Reali et al. 2020). The precession-induced changes in recoils $|V_{\rm p} - V_{\rm np}|$ (where 'p' stands for precession and 'np' stands for no precession), can reach $\sim$3000 km s^{-1} for individual cases. This is consistent with the known sinusoidal variation found in numerical-relativity simulations of 'superkicks' (Brügmann et al. 2008; Gerosa et al. 2018). Around 52 per cent of the merging population experiences an increase in velocity due to precession, and the rest experience a decrease in recoil velocity due to precession. More specifically, 71 per cent of our MBH present recoils that change by at least 10 km s^{-1} when precession is accounted for, 34 per cent of recoil velocities change by at least 100 km s^{-1}, and only 0.7 per cent change by more than 1000 km s^{-1}. Table 1 shows recoil velocity distributions for the different sub-population in our model. As expected, the highest recoil velocities happen for the gas-rich and isotropic spins. The velocities in the gas-rich model are higher because this subset of binaries is consisted of systems with higher mass ratios compared to the gas-poor subset. In the gas-poor subset, we have higher median MBH masses. This means a robust LC hardening that makes the binary merge before a Hubble time.

The recoil velocity distribution for our fiducial model is shown in Fig. 9. For comparison, we also show the velocity distribution that results from assigning spins to all MBHs from the 'aligned' distribution, and from the 'isotropic' distribution (cf. Section 2.4). For all of the distributions in the figure, the spin magnitude, χ, assignment follows the gas dependent criterion given in equation (5). If we assume the 'aligned' distribution, spins are nearly aligned with each other and the orbital angular momentum at the onset of the GW phase. In this case, the recoil velocity distribution peaks at $\sim$140 km s^{-1}. On the other hand, for the 'isotropic' distribution, the recoil velocity distribution peaks at $\sim$700 km s^{-1}, with a large tail of recoils $>$1000 km s^{-1}. Based on our fiducial model, the misaligned portion of the population, 19 per cent of primaries and 10 per cent of secondaries, are assigned a random spin orientation and the rest are assigned spins from the 'aligned' distribution. Therefore, the recoil velocities in the fiducial model lie between a purely 'aligned' and purely 'isotropic' distribution, as shown in Fig. 9. While the fiducial model has a recoil velocity distribution that peaks at around the same value as the aligned distribution, it presents a higher velocity tail that extends to $\sim$3000 km s^{-1}. There are $\sim$12 per cent fiducial systems with a recoil velocity of $\geq$500 km s^{-1} and $\sim$3 per cent systems with a recoil velocity of $\geq$500 km s^{-1}.

Table 1. GW recoil velocity statistics are listed here for our fiducial model (first row in bold) and the eight sub-populations that it is consisted of. Data in this table show percentages evaluated from merged binaries only. The first column denotes whether the host galaxy is gas rich or gas poor (as defined above); this designation determines the initial assignment of BH spin magnitudes in our calculation. The second and third columns distinguish systems in which each BH is aligned or not aligned by the end of the gas-driven phase ($t_{\rm align} < t_{\rm insp}$ versus $t_{\rm align} > t_{\rm insp}$); this determines whether each BH is assigned a spin orientation from the 'aligned' or 'isotropic' distribution. The fourth and fifth columns indicate the median mass ratio q and median binary mass $M_{\rm bin}$ for each sub-population. The sixth column indicates the percentage of merging binaries that fall into each sub-population. The seventh column indicate their median recoil velocity with precession ($v_{\rm np}$). The eighth and ninth columns give the percentage of each sub-population resulting in recoil kicks above 500 and 1000 km s^{-1}, respectively. Note that binaries in gas-rich hosts have more equal mass ratios than those in gas-poor hosts, resulting in somewhat higher recoil velocities for the former. We can also see here that misaligned primaries contribute more to higher recoil velocities. Values are averaged over 10 realizations, with the standard deviations shown for the kick-velocity percentiles in the final two columns.

Host	$\theta_1(\mathbf{r}_{\rm GW})$	$\theta_2(\mathbf{r}_{\rm GW})$	Median q	Median $M_{\rm bin}$ ($M_\odot$)	Per cent of mergers (merged binaries)	Median $v_{\rm p}$ (km s^{-1})	Per cent $v > 500$ km s^{-1} (km s^{-1})	Per cent $v > 1000$ km s^{-1}
Merged binaries	**Fiducial**	**Fiducial**	**0.22**	**4.7×10^7**	**100**	**147**	**12**	**2.6**
Gas rich	Isotropic	Isotropic	0.59	6.4×10^6	0.54	711	65 ± 9.7	34 ± 8.8
Gas rich	Isotropic	Aligned	0.12	1.8×10^7	2.4	248	28 ± 2.9	12 ± 2.6
Gas rich	Aligned	Isotropic	–	–	0.0	–	–	–
Gas rich	Aligned	Aligned	0.36	1.9×10^7	27	189	14 ± 1.2	1.8 ± 0.4
Gas poor	Isotropic	Isotropic	0.042	1.1×10^9	8.1	42.8	21 ± 1.1	9.8 ± 1.2
Gas poor	Isotropic	Aligned	0.077	1.1×10^8	7.9	111	10 ± 1.1	3.1 ± 1.3
Gas poor	Aligned	Isotropic	0.002	1.5×10^9	1.4	0.07	0.0 ± 0	0.0 ± 0
Gas poor	Aligned	Aligned	0.24	5.4×10^7	52	136	10 ± 0.7	1.2 ± 0.2

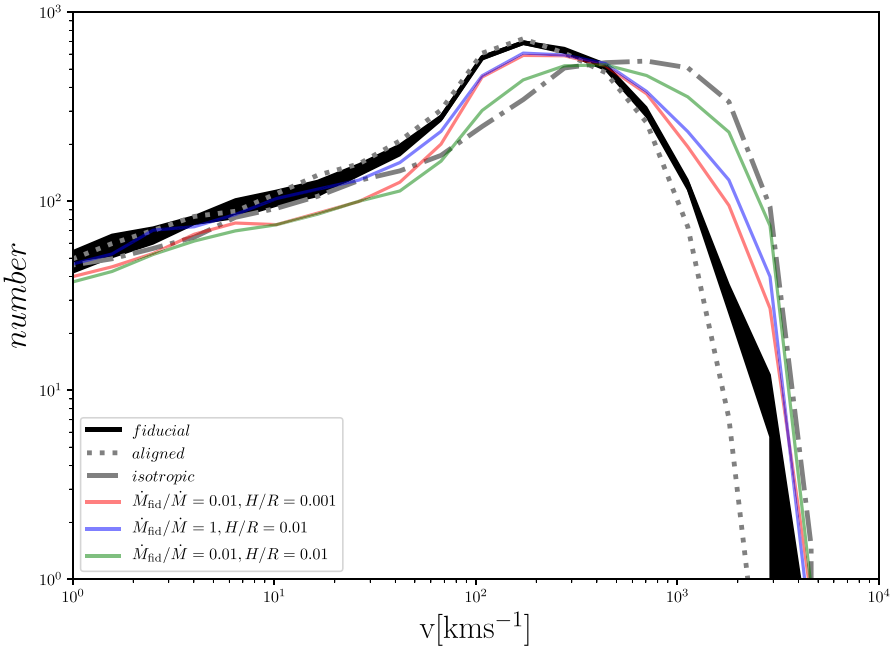

Figure 9. The black solid line indicates GW recoil velocities for the fiducial model, which assigns 'aligned' or 'isotropic' spin-angle distributions based on the alignment time-scales. The shaded area around the fiducial model (apparent at large velocities) indicates the standard deviation over 10 realizations of our model. For comparison, we also include the recoil velocities resulting using entirely the 'aligned' and 'isotropic' distributions (grey dotted and grey dashed dotted, respectively) along with the reduced accretion rate and thick disc models. Greater spin misalignment of the isotropic model yields higher recoil velocities while, on the other hand, for the nearly aligned distribution the recoil velocity distribution peaks at smaller values. The fiducial model, being a combination of the two distributions, sits in between the two extremes, and has a tail of high-velocity recoils extending to ∼3000 km s^{-1}. With the reduced accretion model, the spin orientation becomes more isotropic compared to the fiducial model. Hence, the recoils are pushed to higher values. Higher disc aspect ratio is more efficient and making the distribution isotropic. Therefore, it has slightly higher kick velocities compared to reduced accretion model. Changing both the aspect ratio and the accretion rate will result in even higher kick velocities, as shown in green here.

3.2 Dependence of spin evolution on accretion environment

Because the accretion-disc scale is far smaller than the resolution of Illustris, the simulated Bondi accretion rates are inherently uncertain and may well be overestimated. Although accretion rates could in principle be underestimated, they are Eddington limited and their distribution in Illustris is strongly peaked at the Eddington limit during MBH mergers (Blecha et al. 2016), which is where we focus on in this paper. This makes the overestimate scenario more likely. Combining that with the fact that our results are quite sensitive to accretion rates, we consider alternate models with lower $\dot{m}$ to determine the impact on our results, if in fact these high accretion rates are overestimated during merger events. To this end, we have repeated our calculations with artificially reduced accretion rates

Table 2. Fraction of MBHs with misaligned spins at the start of the GW-dominated phase for our fiducial model (first row, in boldface) and three model variations in which we modify the accretion rate and the aspect ratio of the disc. The 'primary' and 'secondary' columns show the misalignment percentages of the respective MBHs. For both primary and secondary MBHs, spin evolution is strongly affected by changes in the accretion rate and disc aspect ratio. The change in accretion rates modifies both the alignment time-scales and the inspiral time-scales, while the change in aspect ratio modifies the alignment time-scales only. Our fiducial model uses conservative assumptions for the accretion disc, while in other models a large majority of the MBHs are misaligned at the onset of the GW-driven phase.

Disc H/R	Disc $\dot{M}$	Per cent misaligned		Median v ($\mathrm{km\,s^{-1}}$)	Per cent $v > 500\,\mathrm{km\,s^{-1}}$	Per cent $v > 1000\,\mathrm{km\,s^{-1}}$
		Primary	Secondary			
0.001	$\dot{M}_{\mathrm{fid}}$	**19**	**10**	**147**	**12.47**	**2.6**
0.001	$0.01\dot{M}_{\mathrm{fid}}$	48	25	189	19.68	6.32
0.01	$\dot{M}_{\mathrm{fid}}$	48	18	180	20.40	7.43
0.01	$0.01\dot{M}_{\mathrm{fid}}$	79	42	261	31.28	14.03

by a factor of 100. Furthermore, because a significant number of the merging MBHs in Illustris are Eddington-limited at the time of merger (9 per cent), this reduced accretion model variation is effectively testing a scenario where all of these MBHs are low-luminosity rather than high-luminosity AGN. With this reduction factor, 31 per cent of merging MBHs have Eddington ratios $\gtrsim 10^{-3}$, as opposed to 82 per cent with the fiducial model's accretion rates, which are extracted directly from Illustris.

Our results, shown in Table 2, demonstrate that accretion rates strongly influence the alignment and inspiral time-scales of binaries. BP alignment time is inversely proportional to the accretion rate, and thus MBH spins will take longer to align with the disc in systems with low values of $\dot{M}$. In the models with reduced accretion rates, a higher fraction of binaries are misaligned when they enter the GW-driven phase – 79 per cent of primaries and 42 per cent of secondaries for the thicker disc. These fractions are more than three times higher than those in our fiducial model. As the fraction of misaligned MBHs increases, the total spin distribution will begin to resemble a isotropic distribution. Fig. 9 shows the recoil velocity for the reduced accretion model in solid brown and, as expected, this model shows larger recoil velocities compared to the fiducial model. We find that 19.7 per cent and 6.3 per cent of recoils are above 500 and 1000 $\mathrm{km\,s^{-1}}$, respectively.

Table 2 also shows the dependence of alignment on the aspect ratio of the disc. Because the relationship between aspect ratio and accretion rate is somewhat uncertain and may depend on multiple factors (Abramowicz et al. 1988; Nowak 1995; Maccarone 2003; Maccarone & Coppi 2003), we vary these model components independently to span a range of possibilities. The aspect ratio equation only enters the expression for the alignment time-scale. A smaller aspect ratio reduces the alignment time-scales and hence the percentage of misaligned binaries. Table 2 shows that increasing the aspect ratio from 0.001 to 0.01 boosts spin misalignment by more than a factor of 2 for primaries and slightly less than that for secondaries. Such a high percentage of misalignment will make the recoil distribution resemble the full 'isotropic' case. For this model variation, we find that 20 and 7 per cent of recoils are above 500 and 1000 $\mathrm{km\,s^{-1}}$, respectively. The recoil distribution in the large aspect ratio model has the same peak as the reduced accretion model. Finally, a reduction in the accretion rates accompanied by an increase in the aspect ratio will change the distribution most significantly, by driving it closer to the 'isotropic' distribution. With the 79 and 42 per cent misaligned primaries and secondaries, respectively, the percentage of recoils above 500 and 1000 $\mathrm{km\,s^{-1}}$ are 31 and 14 per cent. The peak of the distribution also shifts to $\sim$500 $\mathrm{km\,s^{-1}}$ compared to $\sim$150 $\mathrm{km\,s^{-1}}$ for $\dot{M}_{\mathrm{fid}}/100$ and for the increased aspect ratio $H/R = 0.01$.

For our fiducial model, we have also looked at the correlation of the recoil velocities with galaxy properties such as gas fraction, star formation rates, and the masses of different galaxy components (gas, DM, stars, and black holes). We find that binaries that merge by $z = 0$ have higher host gas fractions. Aside from this, however, the recoil velocities do not show any strong trends with the host galaxy properties. This reflects the fact that only the spin magnitudes in our model have an explicit dependence on host galaxy properties, and the difference between the 'dry-merger' and 'coherent accretion' spin magnitude distributions is relatively minor (see Fig. 4). However, there is an important indirect connection with the host galaxies, namely that gas-poor systems have smaller mass ratios on average, as seen in Table 1. This suggests that in many of these cases there is a satellite merging with a more massive MBH that resides in a gas-poor elliptical galaxy. We plan to further explore the possible dependence of recoil velocities on host galaxy properties in future work.

3.3 Eccentricities

In our binary-inspiral model, we can initialize the sub-resolution MBH binary orbits with non-zero eccentricities. Eccentricity is then modulated in both the LC and GW inspiral phases (Kelley et al. 2017b). We do not attempt to model eccentricity evolution in the DF or CBD stages. Note also that eccentricity evolution is not included in the GW spin precession calculation. Non-zero eccentricity at the start of the GW phase means that we should start the `PRECESSION` code at a smaller radius. In a recent study by (Phukon et al. 2019) this has been shown to not have a significant effect on the overall GR precession. We can none the less consider the effects of precession and eccentricity evolution separately, to characterize their impact on our results. Fig. 10 shows how MBH binary eccentricity evolves during the LC and GW stages of evolution. In general, the LC phase increases the eccentricity of the binaries that are initially slightly eccentric or have unequal masses, while the GW phase rapidly reduces the eccentricity and circularizes the orbit (Peters 1964; Sesana 2010; Merritt 2013; Kelley et al. 2017b).

One outcome of the higher eccentricities in the LC phase is that LC-driven inspiral will dominate down to smaller binary separations. This effect marginally reduces the effective disc radii r_{disc} and increases the number of systems that merge without a CBD phase. In particular, increasing the initial eccentricity at the beginning of the sub-resolution inspiral (beginning at the DF phase) from 0 to 0.9 increases the percentage of the systems with no CBD-dominated phase from 16 to 25 per cent.

We find that varying binary eccentricities does not affect the distribution of recoil velocities in any meaningful way, primarily

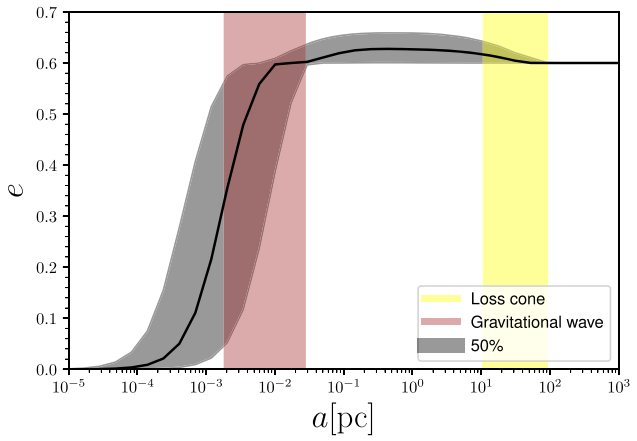

Figure 10. Evolution of binary MBH eccentricity as a function of separation. The eccentricity is evolved in the LC- and GW-dominated phases of our inspiral model. The yellow highlighted region shows the interquartile range for the radii at which binary evolution transitions from DF-dominated to LC-dominated. LC stellar scattering increases the eccentricity. The red highlighted region indicates the interquartile range of radii at which GW hardening begins to dominate. The GW phase leads to a reduction in eccentricity and circularization of the binary.

because no eccentricity evolution occurs during the CBD phase in our model. Thus, BP alignment time-scales and inspiral time-scales do not change, except in so far as the disc radius is modulated by eccentricity evolution in the LC-driven phase. The recoil velocities do not change significantly either; there is negligible change with eccentricity for $e \lesssim 0.5$, while for higher eccentricities, a slight increase is seen in the highest velocity tail of the distribution. The highest 1 per cent of recoil velocities are $\gtrsim$1400 km s^{-1} for $e = 0.5$, versus $\gtrsim$1700 km s^{-1} for $e = 0.8$. This comes from the more isotropic spins for the higher eccentricity. There are 18 and 9 per cent misaligned primaries and secondaries at $e = 0.5$. For $e = 0.8$, the misalingment percentages are 20 and 12 per cent for primaries and secondaries, respectively.

It is worth stressing that residual eccentricity at merger can actually be very important for black hole recoils (Sopuerta, Yunes & Laguna 2007; Sperhake et al. 2020). Here, we are neglecting those effects by construction because the numerical-relativity fitting formula we use is only valid for circular orbits. This is a good approximation because the eccentricity decays quickly before merger (Fig. 10). Eccentricity is also neglected in the spin-precession evolution. We cannot rule out the possibility that the coupled effects of eccentricity and precession could alter the final spin distribution and thus the recoil; further exploration of this is a subject for future work (see Phukon et al. 2019).

3.4 MBH merger rates

The total merger rate, with no delay (i.e. the Illustris merger rate), for all the 9234 binaries from the simulation is 0.53 yr^{-1}. Out of this population, 47 per cent (4269) merge by $z = 0$ in our fiducial model with a merger rate of 0.15 yr^{-1}. Let us recall that these rates are for MBHs with $M > 10^6$ M$_\odot$ and that the mass cut is implemented to avoid dynamical uncertainties regarding MBHs near the seed mass, as described in Section 2. We find that the total merger rate does not depend significantly on the assumed initial eccentricities e, at the beginning of DF phase. The merger rates for $e = 0$ and $e = 0.9$ are 0.14 and 0.16 yr^{-1}, respectively. The dependence on the accretion rate is also minimal. The reduced accretion rate model yields 0.13 yr^{-1} compared to 0.15 yr^{-1} for the fiducial model.

ISA is most sensitive to mergers between binaries with masses $\lesssim$1 M$_\odot$ out to a redshift of $z \sim 20$, with limited sensitivity to more nearby mergers at higher masses ($\lesssim 10^8$ M$_\odot$; e.g. Klein et al. 2016; Amaro-Seoane et al. 2017). We find that 67 per cent of the merged population (2970 binaries) falls within this mass range ($\lesssim$10^8 M$_\odot$), with a corresponding merger rate of 0.1 yr^{-1}. The merger rates quoted here are not equivalent to LISA event rates, as that requires setting a detectability threshold and a consideration of the LISA noise versus binary frequency.

Crucially, these merger rates extracted from the Illustris MBH population will necessarily underestimate the true merger rate, primarily because our analysis is restricted to MBH masses $\geq 10^6$ M$_\odot$ owing to resolution limits. In contrast, semi-analytical models of MBH evolution, which are computationally cheaper compared to large cosmological simulations, often include prescriptions for low-mass MBH seeds ($\sim 10^2$–10^3 M$_\odot$; e.g. Berti et al. 2016; Klein et al. 2016). Such models are therefore able to predict merger rates over essentially the full range of LISA sensitivity, finding merger rates as high as 23 yr^{-1} (Bonetti et al. 2019). Bonetti et al. (2019) also include a model for triple MBH encounters, which are neglected in our analysis, and find that they contribute substantially to the merger rate. Note also that the efficiency of semi-analytical calculations comes at the expense of information about the internal structure of galaxies; these detailed data provided by the Illustris simulation are critical for our models of MBH binary inspiral and spin evolution.

Using Illustris binaries, Katz et al. (2020) reported a merger rate of 0.5–1 yr^{-1}. They made use of a new method for dealing with the uncertainties due to the seeding mechanisms at masses $\lesssim 10^6$ M$_\odot$. Katz et al. (2020) included some, but not all, of the binaries in the mass range 10^5–10^6 M$_\odot$, which we neglected in order to deal with the artificial mergers that were created by the Illustris Friends-of-Friends algorithm near the seed masses, Katz et al. (2020) required all merger constituents to exist for at least one snapshot before merger. They then focus on galaxies that have had their central MBH removed by the re-positioning algorithm. They track the evolution of the galaxy that have lost an MBH in a flyby encounter to ensure it is not artificially seeded again. If the galaxy is seeded at some point after the encounter that seed and all its associated mergers are removed. MBH binaries within this mass range almost doubled their analysed population to 17 535 compared to 9234 in our analysis. Their results are consistent with our findings for $>10^6$ M$_\odot$.

Salcido et al. (2016) presented an MBH merger analysis using the EAGLE, a large cosmological simulation with resolution and volume similar to those of Illustris (Fattahi et al. 2016). Their findings for seed masses similar to Illustris ($M_{\rm seed} = 10^5$ M$_\odot$) yield about 2 mergers per year. Given all of the differences in the numerical techniques and sub-grid models, these results are in reasonable agreement with the Illustris merger rates.

3.5 Characteristics of precessing binaries

The subset of MBH binaries that undergo strong precession is of particular interest for LISA, because these systems will have the largest precession-induced modulation of their GW waveforms, which could potentially be detectable. Because the signal-to-noise ratio required to detect precession depends non-trivially on both the sensitivity curve and the amplitude of precession and nutation, we cannot directly comment on the observability of precessing binaries with LISA. Although a detailed study of precessing GW waveforms

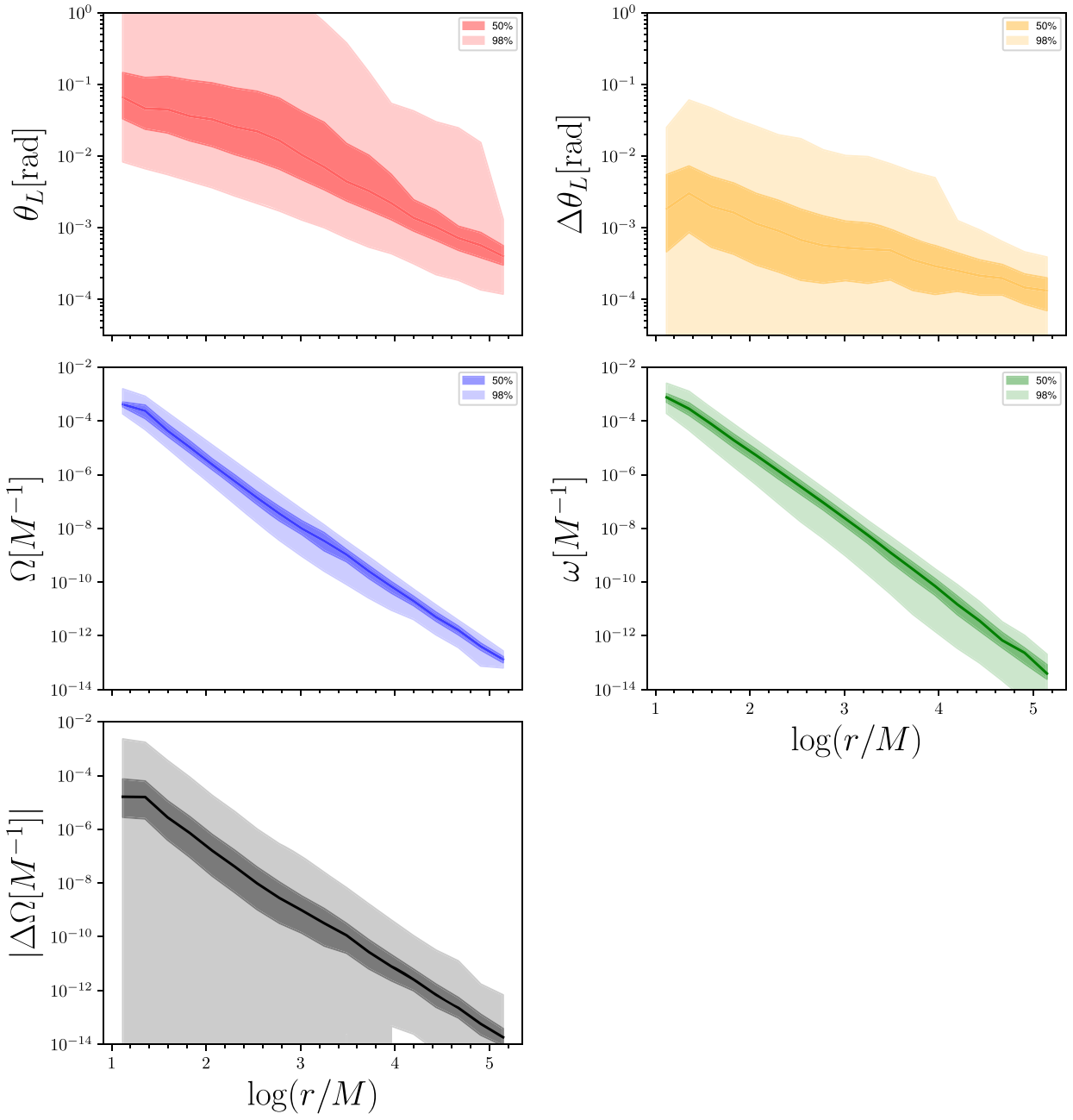

Figure 11. For our population of merging MBH binaries, the evolution of five parameters characterizing GR precession is shown. The five panels show the precession amplitude θ_L (upper left), nutation amplitude $\Delta\theta_L$(upper right), precession frequency Ω (middle left), nutation frequency ω (middle right), and magnitude of oscillation of the precession frequency $|\Delta\Omega|$ (bottom panel). Angles are in radians, and frequencies are in dimensionless M^{-1} units. These quantities are the key spin observables affecting modulation and amplitude of the GW waveform. The light shaded areas show 98 per cent of the data, and the dark shaded areas show the interquartile range.

is beyond the scope of this work, here, we briefly characterize the evolution of key quantities in the GR precession phase.

During the GR precession phase of the evolution, there are five main geometrical quantities that can affect the modulation of the emitted waveform: the precession amplitude θ_L, precession frequency Ω, the nutation amplitude $\Delta\theta_L$, the nutation frequency ω, and the oscillation of the precession frequency due to nutation $\Delta\Omega$ (for details on how these quantities are defined, see Kesden et al. 2015; Gerosa et al. 2015a, 2019; Zhao, Kesden & Gerosa 2017). Fig. 11 shows the evolution of these quantities for the merging MBH binary population as a function of binary separation.

The top left panel in Fig. 11 shows the evolution of the precession amplitude (θ_L) during binary inspiral. Binaries in Fig. 11 indicate all the merged binaries, as we do not explicitly calculate an event rate for mergers in LISA band. At large separations ($a \gtrsim 10^4$ M), the median precession amplitude is small, $\theta_L \lesssim 10^{-3}$ rad. But θ_L generally increases as the binary inspiral progresses, with median values of a few $\times\ 10^{-2}$ to 0.1 rad at $a < 10^3$ M. In addition, a growing tail of large precession amplitudes appears at small separations. About

14 per cent of all merging binaries have a maximum θ_L greater than $\pi/6$, indicating that a small but significant fraction of all merging MBH binaries undergo strong precession. Additionally, ∼5 per cent have very high maximum precession amplitudes of $\theta_L > \pi/2$.

All of these strongly precessing systems have misaligned spins at the onset of the GW-driven phase, originating from the isotropic distribution. In fact, 70 per cent of all such binaries with misaligned spins have a maximum $\theta_L > \pi/6$, and 26 per cent of the misaligned population has a maximum $\theta_L > \pi/2$. The median θ_L before merger for the misaligned population is 0.96 radians, while for the aligned population it is 0.04 radians. Note that θ_L increases as the binary inspiral progresses; thus, the maximum precession amplitude generally occurs at separations near 10M.

The median nutation amplitude ($\Delta\theta_L$; top right panel in Fig. 11) similarly increases with decreasing binary separation, with typical values of a few $\times\ 10^{-4}$ rad at $r \gtrsim 1000$ M to $\sim 10^{-3}$–10^{-2} rad at $r \sim$ 10–100M. The precession and nutation frequencies (Ω and ω, middle row panels in Fig. 11) and $|\Delta\Omega|$ (3rd row panel shown in grey) all increase sharply with decreasing binary separation. Note that $\Delta\Omega$ can be either positive or negative, but its absolute value increases with decreasing binary separation.

A significant fraction of binaries experience strong precession, even in our conservative fiducial model where most binaries have aligned spins prior to merger. This suggests that some binaries could be strongly precessing when they enter the LISA waveband. Our findings therefore provide strong motivation for future work to quantify the detectability of precession signatures in LISA waveforms.

4 DISCUSSION

We study the evolution of spinning MBH binaries in a cosmological framework, considering both gas-driven spin alignment in CBDs and relativistic precession in the GW-dominated regime. The initial conditions for these calculations are the MBH binary masses, separations, accretion rates, and host galaxy properties of merging MBHs from the Illustris cosmological hydrodynamic simulation (e.g. Genel et al. 2014; Vogelsberger et al. 2014a, b; Nelson et al. 2015). MBH binary hardening rates due to dynamical friction, stellar loss-cone scattering, gaseous CBDs, and GWs are modelled as in Kelley et al. (2017a, b). Spin evolution in the gas-driven inspiral phase is based on the Bardeen–Peterson alignment time-scale and the gas properties of the host galaxy. Finally, we model spin precession in the GW-dominated phase using a PN scheme (Gerosa & Kesden 2016) and calculate the GW recoil velocity of the merged MBH.

Our key results can be enumerated as follows:

(i) The fraction of misaligned binaries is non-negligible even in our conservative fiducial model. The misaligned primaries and secondaries represent 19 and 10 per cent, respectively, of the MBH binaries that merge by $z = 0$. This fraction is up to ∼80 per cent for less conservative models with differing assumptions for accretion rate and disc geometry. Thus, gas-driven MBH spin alignment depends strongly on the detailed conditions in the CBD. The spin distribution before merger, and hence the shape of the recoil velocity distribution, is mostly determined by the disc phase of the inspiral.

(ii) The GW phase strongly modifies the $\Delta\Phi$ distribution, which affects recoil velocities. However, the effect on the overall recoil distribution is small, owing to the low percentage of misaligned spins in our fiducial model. None the less, a non-negligible fraction of merging MBHs obtain large recoil velocities. In our conservative fiducial model, more than 12 per cent of merger remnants have recoil velocities >500 km s^{-1}, and more than 3 per cent have velocities >1000 km s^{-1}. This is higher than the escape velocity of most massive galaxies. In our least conservative model, 31 and 14 per cent of recoils have velocities >500 and >1000 km s^{-1}, respectively.

(iii) Strongly precessing systems constitute a significant number of binaries. We find that 14 and 5 per cent of all merging binaries have a maximum precession amplitude $\theta_L > \pi/6$ and $\theta_L > \pi/2$ radians, respectively. In fact, the large majority (70 per cent) of binaries with misaligned spins at the onset of the GW phase have a maximum $\theta_L > \pi/6$, and 26 per cent of misaligned binaries have maximum $\theta_L > \pi/2$. Although we cannot comment directly on the potential detectability of these precessing GW waveforms with LISA, our results strongly motivate future work to quantify the likelihood that such signatures will be observable in the LISA data stream.

(iv) The MBH merger rate from our model is 0.15 mergers per year. Because we are not probing masses $<10^6$ M$_\odot$, the actual LISA detection rate will be higher. Our results are in good agreement with similar recent analysis (e.g. Katz et al. 2020).

Our findings show that there are a significant number of systems with recoil velocities higher than 500 km s^{-1} – larger than the escape velocity of some galaxies. This indicates that MBHs may often be displaced from their host nuclei at least briefly following a merger, and it implies the existence of an intergalactic population of MBHs with no host galaxy (e.g. Volonteri et al. 2003; Madau et al. 2004; Blecha et al. 2011; Gerosa & Sesana 2015; Izquierdo-Villalba et al. 2020); some of these could be observable as offset AGN (e.g. Loeb 2007; Volonteri & Madau 2008; Blecha et al. 2016). Ejected and displaced MBHs could also deflate the subsequent MBH merger rate (Barausse et al. 2020). Volonteri, Gültekin & Dotti (2010) showed that the possibility of ejection is strongly suppressed in gas-rich environments where the spins are more aligned. However, in their study, they do not take into account the general relativistic evolution of spins. Recoil velocities of merged MBHs depend strongly on the spin configurations of the progenitors. We find that, although general relativistic spin precession can strongly affect individual binary spins, it has minimal effect on the overall recoil distribution of merging MBHs. The main factor responsible for the changes in recoil velocities is the BP alignment in the disc-dominated phase.

The efficiency of BP alignment depends strongly on accretion rates and disc aspect ratios. However, in reality these two parameters are also correlated with each other; geometrically thin, radiatively efficient accretion discs are commonly associated with high accretion rates (e.g. Abramowicz et al. 1988). Because we treat these disc parameters independently and assume that the BP effect (equation 2) can be applied to all binaries, it is possible that our model overestimates the role of BP alignment in the CBD-driven phase.

Another potential limitation of our model lies in the implicit assumption that, on average, the MBHs are spun up in gas-rich hosts. This might not always be case, for example when MBH accretion is dominated by chaotic accretion episodes (e.g. King & Pringle 2006; Berti & Volonteri 2008; Fanidakis et al. 2011) or irregular flows caused by angular momentum flips during galaxy mergers (Capelo & Dotti 2017). However, because spin orientations evolve on much shorter time-scales than spin magnitudes, the coherence of larger scale accretion flows is likely to affect the spin magnitudes more than the spin orientations. We recall that our results depend very minimally on the choice of spin magnitudes. Our assignments of the spin magnitudes could also be improved by considering a model in which the spin evolution due to accretion is explicitly traced through the CBD phase. We refer the reader to Dubois, Volonteri & Silk (2014) and Bustamante & Springel (2019) for a more in depth discussion of accretion and merger effects on the spins. In addition

to that we have also not considered the case of anti-alignment of the disc and MBH. Depending on the mass of the MBH and the disc mass the accretion could be episodic and the disc might align or anti-align with MBH. This can lead to either spin-up or spin-down of the MBH (Fiacconi, Sijacki & Pringle 2018).

In the GW-dominated phase, we use a PN scheme that does not evolve the binary eccentricities; the analytical calculation of eccentricity evolution is done separately for the GW phase. This is a reasonable approximation as GW tend to circularize binaries on a time-scale which is shorter than the inspiral time (Peters 1964, see also Fig. 10). Additionally, Phukon et al. (2019) have recently shown that eccentricity is subdominant in the spin morphology evolution of MBH binaries. We hope to include a treatment of spinning eccentric binaries in future work.

When the MBH binary inspiral time is longer than the typical time between galaxy mergers, a triple MBH system may form. Kelley et al. (2017a) find that a non-negligible fraction of binaries are still unmerged when a subsequent galaxy merger occurs, but as in that work, we do not attempt to model triple MBH systems here. Triples may not only affect eccentricities but also have important consequences for merger rates. In a triple system, the lightest MBH can get ejected out of the system and accelerate the shrinking of the binary separation (Hills 1975). Alternatively, a third MBH can settle into an outer semicircular orbit and form a hierarchical configuration. The outer MBH can then accelerate the hardening of the inner binary (Kozai 1962; Lidov 1962; Blaes, Lee & Socrates 2002). These factors can increase the overall merger rates (e.g. Biava et al. 2019; Bonetti et al. 2019). Kozai–Lidov oscillations between eccentricity and inclination of the inner binary can also lead to large spin misalignments (Liu & Lai 2018; Rodriguez & Antonini 2018; Liu, Lai & Wang 2019).

In summary, our results demonstrate that MBH spins are a crucial aspect of MBH binary evolution, which will impact the observability of MBH binaries as GW and multimessenger sources for LISA. We find that misaligned spins are not a rare occurrence over cosmic time, suggesting that large recoil velocities may reduce the MBH merger rate somewhat and produce a population of offset or wandering MBHs. Some of these may be observable as offset AGN. The misaligned binary population in our models also suggests that some binaries may be strongly precessing in the LISA band, which could potentially be detected in their GW waveforms. Any such detections would place strong constraints on MBH spins and provide direct confirmation of GR precession. Precessing, accreting binaries could also produce unique electromagnetic signatures such as precessing jets (e.g. Gower et al. 1982; Krause et al. 2019) or the shape and variability of Fe Kα profiles (Yu & Lu 2001). Future work to refine and quantify these predictions in advance of LISA will therefore provide key information about the GW event rate and source characteristics.

ACKNOWLEDGEMENTS

We would like to thank the anonymous referee for their helpful suggestions that have improved the quality of this manuscript. We would also like to thank Pedro Capello, Chiara Mingarelli, Dan D'Orazio, and Marta Volonteri for insightful comments and discussions. In addition, we would like to thank the attendees of the LISA Symposium (2018), BASS workshop (2019), and JSI workshop (2019) for fruitful suggestions. This work made use of the PYTHON programming language (Rossum & De Boer 1991), and its NUMPY (van der Walt, Colbert & Varoquaux 2011), SCIPY (Virtanen et al. 2020), and MATPLOTLIB (Hunter 2007) packages along with Jupyter notebooks (Kluyver et al. 2016). LB acknowledges support from NSF Grant No. AST-1909933. DG is supported by European Union's H2020 ERC Starting Grant No. 945155–GWmining, Leverhulme Trust Grant No. RPG-2019-350, and Royal Society Grant No. RGS-R2-202004. MK is supported by NSF Grants No. PHY-1607031 and PHY-2011977. Computational work was performed on the University of Florida Hipergator cluster, Harvard's Odyssey cluster, the University of Brimingham BlueBEAR cluster, the Athena cluster at HPC Midlands + funded by EPSRC Grant No. EP/P020232/1, and the Maryland Advanced Research Computing Center (MARCC).

DATA AVAILABILITY

The data underlying this article will be shared on reasonable request to the corresponding author.

REFERENCES

Abramowicz M. A., Czerny B., Lasota J. P., Szuszkiewicz E., 1988, ApJ, 332, 646
Amaro-Seoane P. et al., 2017
Antonini F., Merritt D., 2012, ApJ, 745, 83
Apostolatos T. A., Cutler C., Sussman G. J., Thorne K. S., 1994, Phys. Rev. D, 49, 6274
Armitage P. J., Natarajan P., 2002, ApJ, 567, L9
Artymowicz P., Lubow S. H., 1996, ApJ, 467, L77
Barausse E., 2012, MNRAS, 423, 2533
Barausse E., Dvorkin I., Tremmel M., Volonteri M., Bonetti M., 2020, ApJ, 904, 16
Bardeen J. M., 1970, Nature, 226, 64
Bardeen J. M., Petterson J. A., 1975, ApJ, 195, L65
Barnes J. E., 1992, ApJ, 393, 484
Batcheldor D., Robinson A., Axon D. J., Perlman E. S., Merritt D., 2010, ApJ, 717, L6
Begelman M. C., Blandford R. D., Rees M. J., 1980, Nature, 287, 307
Bekenstein J. D., 1973, ApJ, 183, 657
Bellovary J., Volonteri M., Governato F., Shen S., Quinn T., Wadsley J., 2011, ApJ, 742, 13
Berger M. J., Colella P., 1989, J. Comput. Phys., 82, 64
Berti E., Volonteri M., 2008, ApJ, 684, 822
Berti E., Kesden M., Sperhake U., 2012, Phys. Rev. D, 85, 124049
Berti E., Sesana A., Barausse E., Cardoso V., Belczynski K., 2016, Phys. Rev. Lett., 117, 101102
Biava N., Colpi M., Capelo P. R., Bonetti M., Volonteri M., Tamfal T., Mayer L., Sesana A., 2019, MNRAS, 487, 4985
Blaes O., Lee M. H., Socrates A., 2002, ApJ, 578, 775
Blanchet L., 2014, Living Rev. Relativ., 17, 2
Blecha L., Loeb A., 2008, MNRAS, 390, 1311
Blecha L., Cox T. J., Loeb A., Hernquist L., 2011, MNRAS, 412, 2154
Blecha L., Civano F., Elvis M., Loeb A., 2013, MNRAS, 428, 1341
Blecha L. et al., 2016, MNRAS, 456, 961
Bogdanović T., Reynolds C. S., Miller M. C., 2007, ApJ, 661, L147
Bogdanović T., Eracleous M., Sigurdsson S., 2009, ApJ, 697, 288
Bonetti M., Sesana A., Haardt F., Barausse E., Colpi M., 2019, MNRAS, 486, 4044
Bowen D. B., Campanelli M., Krolik J. H., Mewes V., Noble S. C., 2017, ApJ, 838, 42
Brügmann B., González J. A., Hannam M., Husa S., Sperhake U., 2008, Phys. Rev. D, 77, 124047
Burke-Spolaor S., 2015, Gravitational-Wave Detection and Astrophysics with Pulsar Timing Arrays, preprint (arXiv:1511.07869)
Bustamante S., Springel V., 2019, MNRAS, 490, 4133
Calderón Bustillo J., Clark J. A., Laguna P., Shoemaker D., 2018, Phys. Rev. Lett., 121, 191102
Campanelli M., Lousto C. O., Zlochower Y., Merritt D., 2007a, Phys. Rev. Lett., 98, 231102

Campanelli M., Lousto C., Zlochower Y., Merritt D., 2007b, ApJ, 659, L5
Capelo P. R., Dotti M., 2017, MNRAS, 465, 2643
Chandrasekhar S., 1942, Principles of Stellar Dynamics. Chicago, Ill., The University of Chicago press, Chicago
Chandrasekhar S., 1943, ApJ, 97, 255
Chiaberge M. et al., 2017, A&A, 600, A57
Civano F. et al., 2010, ApJ, 717, 209
Civano F. et al., 2012, ApJ, 752, 49
Detweiler S., 1979, ApJ, 234, 1100
Di Matteo T., Springel V., Hernquist L., 2005, Nature, 433, 604
D'Orazio D. J., Haiman Z., MacFadyen A., 2013, MNRAS, 436, 2997
Dotti M., Volonteri M., Perego A., Colpi M., Ruszkowski M., Haardt F., 2010, MNRAS, 402, 682
Dubois Y., Volonteri M., Silk J., 2014, MNRAS, 440, 1590
Duffell P. C., D'Orazio D., Derdzinski A., Haiman Z., MacFadyen A., Rosen A. L., Zrake J., 2020, ApJ, 901, 25
Escala A., Larson R. B., Coppi P. S., Mardones D., 2005, ApJ, 630, 152
Fanidakis N., Baugh C. M., Benson A. J., Bower R. G., Cole S., Done C., Frenk C. S., 2011, MNRAS, 410, 53
Farris B. D., Duffell P., MacFadyen A. I., Haiman Z., 2014, ApJ, 783, 134
Fattahi A. et al., 2016, MNRAS, 457, 844
Fiacconi D., Sijacki D., Pringle J. E., 2018, MNRAS, 477, 3807
Fitchett M. J., 1983, MNRAS, 203, 1049
Genel S. et al., 2014, MNRAS, 445, 175
Gerosa D., Kesden M., 2016, Phys. Rev. D, 93, 124066
Gerosa D., Moore C. J., 2016, Phys. Rev. Lett., 117, 011101
Gerosa D., Sesana A., 2015, MNRAS, 446, 38
Gerosa D., Kesden M., Berti E., O'Shaughnessy R., Sperhake U., 2013, Phys. Rev. D, 87, 104028
Gerosa D., Kesden M., Sperhake U., Berti E., O'Shaughnessy R., 2015a, Phys. Rev. D, 92, 064016
Gerosa D., Veronesi B., Lodato G., Rosotti G., 2015b, MNRAS, 451, 3941
Gerosa D., Hébert F., Stein L. C., 2018, Phys. Rev. D, 97, 104049
Gerosa D., Lima A., Berti E., Sperhake U., Kesden M., O'Shaughnessy R., 2019, Class. Quantum Gravity, 36, 105003
Gerosa D., Rosotti G., Barbieri R., 2020, MNRAS, 496, 3060
Gingold R. A., Monaghan J. J., 1977, MNRAS, 181, 375
González J. A., Sperhake U., Brügmann B., Hannam M., Husa S., 2007a, Phys. Rev. Lett., 98, 091101
González J. A., Hannam M., Sperhake U., Brügmann B., Husa S., 2007b, Phys. Rev. Lett., 98, 231101
Gould A., Rix H.-W., 2000, ApJ, 532, L29
Gower A. C., Gregory P. C., Unruh W. G., Hutchings J. B., 1982, ApJ, 262, 478
Gualandris A., Merritt D., 2008, ApJ, 678, 780
Gültekin K. et al., 2009, ApJ, 698, 198
Günther R., Kley W., 2002, A&A, 387, 550
Haiman Z., Kocsis B., Menou K., 2009, ApJ, 700, 1952
Hanawa T., Ochi Y., Ando K., 2010, ApJ, 708, 485
Hayasaki K., Mineshige S., Ho L. C., 2008, ApJ, 682, 1134
Hayward C. C., Narayanan D., Kereš D., Jonsson P., Hopkins P. F., Cox T. J., Hernquist L., 2013, MNRAS, 428, 2529
Heckman T. M., Krolik J. H., Moran S. M., Schnittman J., Gezari S., 2009, ApJ, 695, 363
Hernquist L., 1992, ApJ, 400, 460
Hills J. G., 1975, AJ, 80, 809
Hinshaw G. et al., 2013, ApJS, 208, 19
Hopkins P. F., Hernquist L., Hayward C. C., Narayanan D., 2012, MNRAS, 425, 1121
Hunter J. D., 2007, Comput. Sci. Eng., 9, 90
Izquierdo-Villalba D., Bonoli S., Dotti M., Sesana A., Rosas-Guevara Y., Spinoso D., 2020, MNRAS, 495, 4681
Katz M. L., Kelley L. Z., Dosopoulou F., Berry S., Blecha L., Larson S. L., 2020, MNRAS, 491, 2301
Kelley L. Z., Blecha L., Hernquist L., 2017a, MNRAS, 464, 3131
Kelley L. Z., Blecha L., Hernquist L., Sesana A., Taylor S. R., 2017b, MNRAS, 471, 4508
Kelley L. Z., Blecha L., Hernquist L., Sesana A., Taylor S. R., 2018, MNRAS, 477, 964
Kelley L. Z., Haiman Z., Sesana A., Hernquist L., 2019, MNRAS, 485, 1579
Kesden M., Sperhake U., Berti E., 2010a, Phys. Rev. D, 81, 084054
Kesden M., Sperhake U., Berti E., 2010b, ApJ, 715, 1006
Kesden M., Gerosa D., O'Shaughnessy R., Berti E., Sperhake U., 2015, Phys. Rev. Lett., 114, 081103
King A. R., Kolb U., 1999, MNRAS, 305, 654
King A. R., Pringle J. E., 2006, MNRAS, 373, L90
Klein A. et al., 2016, Phys. Rev. D, 93, 024003
Kluyver T. et al., 2016 , in Loizides F., Scmidt B., eds, Positioning and Power in Academic Publishing: Players, Agents and Agendas. IOS Press, Amsterdam, p. 87
Komossa S., 2012, Adv. Astron., 2012, 364973
Komossa S., Zhou H., Lu H., 2008, ApJ, 678, L81
Kormendy J., Ho L. C., 2013, ARA&A, 51, 511
Kormendy J., Fisher D. B., Cornell M. E., Bender R., 2009, ApJS, 182, 216
Koss M. et al., 2014, MNRAS, 445, 515
Kozai Y., 1962, AJ, 67, 591
Krause M. G. H. et al., 2019, MNRAS, 482, 240
Lehner L., Pretorius F., 2014, ARA&A, 52, 661
Libeskind N. I., Cole S., Frenk C. S., Helly J. C., 2006, MNRAS, 368, 1381
Lidov M. L., 1962, Planet. Space Sci., 9, 719
Liu B., Lai D., 2018, ApJ, 863, 68
Liu B., Lai D., Wang Y.-H., 2019, ApJ, 881, 41
Lodato G., Gerosa D., 2013, MNRAS, 429, L30
Lodato G., Pringle J. E., 2006, MNRAS, 368, 1196
Lodato G., Nayakshin S., King A. R., Pringle J. E., 2009, MNRAS, 398, 1392
Loeb A., 2007, Phys. Rev. Lett., 99, 041103
Lommen A. N., 2015, Rep. Prog. Phys., 78, 124901
Lousto C. O., Zlochower Y., 2008, Phys. Rev. D, 77, 044028
Lousto C. O., Zlochower Y., 2013, Phys. Rev. D, 87, 084027
Lousto C. O., Zlochower Y., Dotti M., Volonteri M., 2012, Phys. Rev. D, 85, 084015
Lucy L. B., 1977, AJ, 82, 1013
Maccarone T. J., 2003, A&A, 409, 697
Maccarone T. J., Coppi P. S., 2003, MNRAS, 338, 189
MacFadyen A. I., Milosavljević M., 2008, ApJ, 672, 83
Madau P., Quataert E., 2004, ApJ, 606, L17
Madau P., Rees M. J., Volonteri M., Haardt F., Oh S. P., 2004, ApJ, 604, 484
Magorrian J., Tremaine S., 1999, MNRAS, 309, 447
Martin R. G., Pringle J. E., Tout C. A., 2007, MNRAS, 381, 1617
Martin R. G., Pringle J. E., Tout C. A., 2009, MNRAS, 400, 383
Merritt D., 2013, Class. Quantum Gravity, 30, 244005
Merritt D., Rezzolla L., 2013, Class. Quantum Gravity, 30, 240301
Merritt D., Milosavljević M., Favata M., Hughes S. A., Holz D. E., 2004, ApJ, 607, L9
Merritt D., Storchi-Bergmann T., Robinson A., Batcheldor D., Axon D., Cid Fernandes R., 2006, MNRAS, 367, 1746
Mingarelli C. M. F., Grover K., Sidery T., Smith R. J. E., Vecchio A., 2012, Phys. Rev. Lett., 109, 081104
Miranda R., Muñoz D. J., Lai D., 2017, MNRAS, 466, 1170
Moody M. S. L., Shi J.-M., Stone J. M., 2019, ApJ, 875, 66
Mould M., Gerosa D., 2020, Phys. Rev. D, 101, 124037
Muñoz D. J., Lai D., 2016, ApJ, 827, 43
Muñoz D. J., Miranda R., Lai D., 2019, ApJ, 871, 84
Muñoz D. J., Lai D., Kratter K., Mirand a R., 2020, ApJ, 889, 114
Natarajan P., Pringle J. E., 1998, ApJ, 506, L97
Nelson D. et al., 2015, Astron. Comput., 13, 12
Niemi S.-M., Somerville R. S., Ferguson H. C., Huang K.-H., Lotz J., Koekemoer A. M., 2012, MNRAS, 421, 1539
Nowak M. A., 1995, PASP, 107, 1207
Ogilvie G. I., 1999, MNRAS, 304, 557
Perego A., Dotti M., Colpi M., Volonteri M., 2009, MNRAS, 399, 2249
Peres A., 1962, Phys. Rev., 128, 2471
Peters P. C., 1964, Phys. Rev., 136, 1224
Phukon K. S., Gupta A., Bose S., Jain P., 2019, Phys. Rev. D, 100, 124008
Rafikov R. R., 2016, ApJ, 827, 111

Ragusa E., Lodato G., Price D. J., 2016, MNRAS, 460, 1243
Reali L., Mould M., Gerosa D., Varma V., 2020, Class. Quantum Gravity, 37, 225005
Robinson A., Young S., Axon D. J., Kharb P., Smith J. E., 2010, ApJ, 717, L122
Rodriguez C. L., Antonini F., 2018, ApJ, 863, 7
Roedig C., Sesana A., Dotti M., Cuadra J., Amaro-Seoane P., Haardt F., 2012, A&A, 545, A127
Roos N., 1981, A&A, 104, 218
Rossum G. V., De Boer J., 1991, Interactively testing remote servers using the Python programming language. Centrum Wiskunde and Informatica, Amsterdam
Ryan G., MacFadyen A., 2017, ApJ, 835, 199
Salcido J., Bower R. G., Theuns T., McAlpine S., Schaller M., Crain R. A., Schaye J., Regan J., 2016, MNRAS, 463, 870
Sanders D. B., Mirabel I. F., 1996, ARA&A, 34, 749
Savonije G. J., Papaloizou J. C. B., Lin D. N. C., 1994, MNRAS, 268, 13
Sazhin M. V., 1978, Sov. Astron., 22, 36
Scheuer P. A. G., Feiler R., 1996, MNRAS, 282, 291
Schnittman J. D., 2004, Phys. Rev. D, 70, 124020
Schnittman J. D., 2007, ApJ, 667, L133
Sesana A., 2010, ApJ, 719, 851
Sesana A., Volonteri M., Haardt F., 2007, MNRAS, 377, 1711
Sesana A., Haardt F., Madau P., 2008, ApJ, 686, 432
Sesana A., Volonteri M., Haardt F., 2009, Class. Quantum Gravity, 26, 094033
Shakura N. I., Sunyaev R. A., 1973, A&A, 500, 33
Shapiro S. L., 2005, ApJ, 620, 59
Shi J.-M., Krolik J. H., 2015, ApJ, 807, 131
Shi J.-M., Krolik J. H., Lubow S. H., Hawley J. F., 2012, ApJ, 749, 118
Sijacki D., Springel V., Haehnelt M. G., 2011, MNRAS, 414, 3656
Sijacki D., Vogelsberger M., Genel S., Springel V., Torrey P., Snyder G. F., Nelson D., Hernquist L., 2015, MNRAS, 452, 575
Siwek M. S., Kelley L. Z., Hernquist L., 2020, MNRAS, 498, 537
Somerville R. S., Davé R., 2015, ARA&A, 53, 51
Sopuerta C. F., Yunes N., Laguna P., 2007, ApJ, 656, L9
Sperhake U., Rosca-Mead R., Gerosa D., Berti E., 2020, Phys. Rev. D, 101, 024044
Springel V., 2010, MNRAS, 401, 791
Springel V., Di Matteo T., Hernquist L., 2005, MNRAS, 361, 776
Tang Y., MacFadyen A., Haiman Z., 2017, MNRAS, 469, 4258
Tang Y., Haiman Z., MacFadyen A., 2018, MNRAS, 476, 2249
Tremaine S., Davis S. W., 2014, MNRAS, 441, 1408
van der Walt S., Colbert S. C., Varoquaux G., 2011, Comput. Sci. Eng., 13, 22
Varma V., Isi M., Biscoveanu S., 2020, Phys. Rev. Lett., 124, 101104
Virtanen P. et al., 2020, Nat. Methods, 17, 261
Vogelsberger M., Genel S., Sijacki D., Torrey P., Springel V., Hernquist L., 2013, MNRAS, 436, 3031
Vogelsberger M. et al., 2014a, MNRAS, 444, 1518
Vogelsberger M. et al., 2014b, Nature, 509, 177
Volonteri M., Madau P., 2008, ApJ, 687, L57
Volonteri M., Haardt F., Madau P., 2003, ApJ, 582, 559
Volonteri M., Madau P., Quataert E., Rees M. J., 2005, ApJ, 620, 69
Volonteri M., Lodato G., Natarajan P., 2008, MNRAS, 383, 1079
Volonteri M., Gültekin K., Dotti M., 2010, MNRAS, 404, 2143
Volonteri M. et al., 2020, MNRAS, 498, 2219
Will C. M., 2016, Gravity: Where Do We Stand? Gravity: Newtonian, Post-Newtonian, and General Relativistic. Springer International Publishing Switzerland, Switzerland, p. 9
Yu Q., Lu Y., 2001, A&A, 377, 17
Zhao X., Kesden M., Gerosa D., 2017, Phys. Rev. D, 96, 024007

This paper has been typeset from a TEX/LATEX file prepared by the author.